arXiv:0707.4668v2 [cond-mat.other] 2 Aug 2007

Atomic lattice excitons: from condensates to crystals

A. Kantian[1,2], A. J. Daley[1,2], P. Törmä[3], P. Zoller[1,2]

[1] Institute for Quantum Optics and Quantum Information of the Austrian Academy of Sciences, A-6020 Innsbruck, Austria
[2] Institute for Theoretical Physics, University of Innsbruck, A-6020 Innsbruck, Austria
[3] Nanoscience Center, Department of Physics, P.O. Box 35, FIN-40014 University of Jyväskylä, Finland

E-mail: Adrian.Kantian@uibk.ac.at

Abstract. We discuss atomic lattice excitons (ALEs), bound particle-hole pairs formed by fermionic atoms in two bands of an optical lattice. Such a system provides a clean setup to study fundamental properties of excitons, ranging from condensation to exciton crystals (which appear for a large effective mass ratio between particles and holes). Using both mean-field treatments and 1D numerical computation, we discuss the properities of ALEs under varying conditions, and discuss in particular their preparation and measurement.

PACS numbers: 03.75.Ss, 71.35.-y, 42.50.-p

1. Introduction

Excitons, the bound state of a fermionic particle and a fermionic hole, belong to the most basic excitations in any system of fermionic particles confined in the band structure of a periodic potential [1, 2]. In a semiconductor, metastable excitons are created by optically pumping electrons from the valence to the conduction band, and Coulomb repulsion between the electrons then leads to the formation of a bound state of the electron with the hole it left behind. At sufficiently low temperatures, the approximately bosonic statistics of the composite objects give rise to a superfluid state corresponding to a condensate of excitons [1, 2, 3, 4, 5, 6, 7, 8, 9, 10].

In the present work we investigate the properties of bound particle-hole pairs of fermionic atoms confined in an optical lattice, where two-particle interactions are provided by collisional processes between atoms [11, 12, 13, 14], or Atomic Lattice Excitons (ALEs) [15]. Optical Lattice systems [14, 16, 17, 18, 19, 20, 21, 22, 23], have emerged as a very attractive tool for the study of many-body lattice models (see, e.g., [24, 25, 26, 27, 28, 29, 30] particularly because of the high degree of available control over system parameters (e.g., control over interactions using Feshbach resonances [31, 32, 33, 34]. These systems also allow for a wide range of measurement techniques, giving access to quantities including momentum and quasimomentum distribution, and higher-order correlation functions via noise correlation measurements [35, 36, 37].

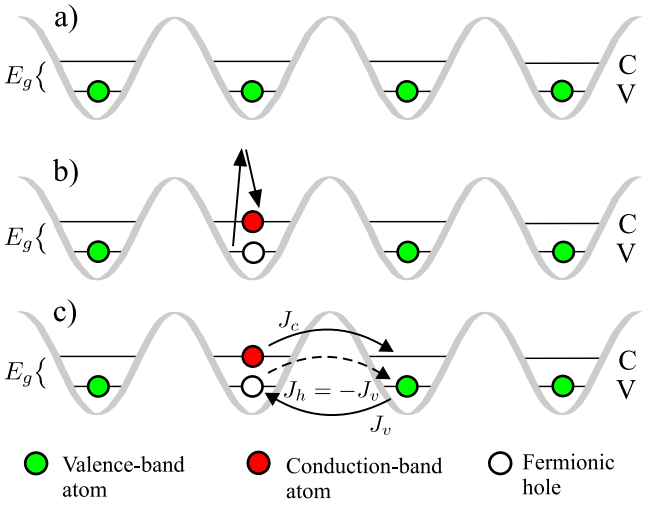


Figure 1. Atomic Lattice Excitons (ALEs): (a) ALEs can be prepared from a fermionic band insulator, with one atom per site in the valence band (denoted V). (b) Pairs of conduction band atoms and valence band holes are created by transferring valence band atoms to the conduction band (denoted C), which is separated from the valence band by the band gap energy E_g. c) Particle-hole pairs move by tunnelling of the conduction-band atom with rate J_c and back tunnelling of a valence-band atom with rate J_v, which corresponds to co-tunnelling of the hole. Co-tunnelling occurs because of the interband atom-atom repulsion U. Thus, atom-hole pairs move together, forming the exciton.

ALEs constitute a novel realisation of excitons, allowing fundamental aspects of excitons as composite objects and as an interacting many body system to be investigated in a particularly clean and controlled setting. In fact, the many body physics represented by ALEs corresponds closely to the basic theoretical models, which have been developed in seminal work in the context of exciton condensates in semiconductors physics, focusing mainly on many body physics of excitons as interacting composite objects of two fermionic electron-hole constituents. A semiconductor environment constitutes, of course, a much more complex system with coupling to other degrees of freedom, e.g., lattice phonons and vacuum modes of the radiation field, which are essentially absent in atomic lattices. Furthermore, additional parameter regimes can be accessed for ALEs, producing quantum phases that are not normally observed in semiconductor systems. This includes, for example, the formation of exciton crystalline structures in regimes where the effective mass of particles and holes on the lattice are substantially different.

In the simplest case, ALEs can be formed in a system of spin-polarised fermions in a optical lattice, where the lowest Bloch band (called the *valence* band) is initially fully occupied (figure 1a). This can be set up in 1D, 2D or 3D, although in this article we will primarily concentrate on the 1D case. This is both the conceptually simplest case as only a single excited Bloch band needs to be considered, and also provides interesting analogies to the possible formation of excitons in quantum wires. The lattice is assumed to be sufficiently deep for a tight-binding approximation [16] to be valid for the first two Bloch bands, which are separated by the band gap E_g. Atomic lattice excitons (ALEs) are created from the ground state by exciting atoms with a

laser driven Raman process into the next highest Bloch band (called the *conduction* band), where they have a tunnelling rate J_c. The excitation leaves a fermionic hole in the valence band, (figure 1b), moving with hopping rate $J_h = -J_v$, where J_v is the valence band hopping rate of the atoms. While spin-polarised fermionic atoms have, by symmetry, no s-wave scattering, a repulsive collisional interaction U can be generated between conduction and valence-band atoms in the same lattice site (e.g., by using an off-resonant Raman transition to mix in some component of a different spin state for particles in one of the two bands.). This on-site repulsion, in turn, gives rise to an effective attraction between conduction-band atoms and holes.

In this work we investigate ALEs, applying both mean-field theory and exact numerical calculations in 1D. We derive the Fermi-Hubbard Model description of ALEs, and then discuss both single ALEs (Sec. 2A) and interaction between two ALEs (Sec. 2B). In particular, interactions between long-lived ALEs, which due to the large effective mass ratio between particles and holes can be analysed in a Born-Oppenheimer approximation, are characterised by a finite range repulsion. In Sec. 3 we then discuss the resulting many-body phases, including ALE condensates, and a crystal phase that arises from the effective long-range interactions. We discuss how the properties of these phases can be measured using RF Spectroscopy and noise correlation techniques (Sec. 4), and discuss schemes to prepare well-defined filling factors of excitons in a low energy many-body state in an optical lattice (Sec. 5). We give a summary in Sec. 6. In Appendix A we provide extra details of our solution for a single exciton on the lattice, while in Appendix B we detail the solution to the problem of N static lattice impurities that underlie our Born-Oppenheimer approximation. Finally, in Appendix C we provide additional information about the general treatment of excition condensation.

2. Atomic lattice excitons (ALEs)

We consider a gas of ALEs, formed in an optical lattice that is sufficiently deep for a tight-binding approximation [16] to be valid for the first two Bloch bands, which are separated by the band gap E_g. If the lattice is isotropic or near-isotropic, there will be degenerate lowest excited p-bands, as discussed in [27]. In this paper we focus on excitons that are tightly confined in two dimensions so that we consider excitons in 1D, and will also give mean-field results that are applicable to excitons in 2D or 3D with strong anisotropies so that the p-band degeneracy is lifted, and one of the bands can be chosen as the conduction band. In the conduction band, atoms have a tunnelling rate $J_c^{\mathbf{X}\mathbf{X}'}$ between neighbouring sites with lattice vectors $\mathbf{x}$ and $\mathbf{x}'$ (these tunnelling rates can, in general, be anisotropic). The excitation then leaves a fermionic hole in the valence band, (figure 1b), moving with hopping rate $J_h^{\mathbf{X}\mathbf{X}'} = -J_v^{\mathbf{X}\mathbf{X}'}$, where $J_v^{\mathbf{X}\mathbf{X}'}$ is the valence band hopping rate of the atoms between neighbouring sites. It is convenient to expand the field operators of the lattice-confined fermions in the localised Wannier modes $w^{\{c,v\}}(\mathbf{r}-\mathbf{x})$ and the corresponding annihilation operators $c_{\mathbf{x}}^{\{c,v\}}$ of conduction and valence band respectively [16]

$$\psi^{\{c,v\}}(\mathbf{r}) = \sum_{\mathbf{x}} c_{\mathbf{x}}^{\{c,v\}} w^{\{c,v\}}(\mathbf{r}-\mathbf{x}), \tag{1}$$

where $\mathbf{x} = a(x_1, \ldots, x_D)$, $(x_1, \ldots, x_D) \in \mathbb{Z}^D$ and a is the lattice spacing.

A repulsive interaction U between conduction and valence-band atoms in the same lattice site can be generated as discussed in sec. 1, which then gives rise to

an effective attraction between conduction-band atoms and holes. A Hamiltonian describing the interacting populations of atoms in two bands can be obtained by inserting the decomposition 1 into the two-species Hamiltonian in second quantization. We obtain a repulsive two-species Hubbard-Hamiltonian,

$$H = -\sum_{\langle \mathbf{x}\mathbf{x}'\rangle} J_c^{\mathbf{x}\mathbf{x}'} c_{\mathbf{x}}^\dagger c_{\mathbf{x}'} - \sum_{\langle \mathbf{y}\mathbf{y}'\rangle} J_v^{\mathbf{y}\mathbf{y}'} b_{\mathbf{y}}^\dagger b_{\mathbf{y}'} + U \sum_{\mathbf{x}} c_{\mathbf{x}}^\dagger b_{\mathbf{x}}^\dagger b_{\mathbf{x}} c_{\mathbf{x}} \tag{2}$$

where $c_{\mathbf{x}}^\dagger$ and $b_{\mathbf{x}}^\dagger$ are atom creation operators on lattice site $\mathbf{x}$ in conduction and valence-band respectively, obetying the usual fermionic commutation relations. This Hamiltonian is valid in the limit where $U, J_c, J_v \ll E_g$, where E_g is the band gap. This is well fulfilled by typical experimental parameters. Note that terms involving transfer of particles from one band to another do not appear because of this condition, and therefore the total number of valence band atoms and the total number of conduction band atoms are conserved separately.

Holes appear through the introduction of fermionic hole creation operators $d_{\mathbf{x}}^\dagger$ in the lower band by the definition $d_{\mathbf{x}}^\dagger = b_{\mathbf{x}}$. This trivial substitution yields the particle-hole Hamiltonian

$$H = -\sum_{\langle xx'\rangle} J_p^{\mathbf{x}\mathbf{x}'} c_{\mathbf{x}}^\dagger c_{\mathbf{x}'} - \sum_{\langle \mathbf{y}\mathbf{y}'\rangle} J_h^{\mathbf{x}\mathbf{x}'} d_{\mathbf{y}}^\dagger d_{\mathbf{y}'} - U \sum_{\mathbf{x}} c_{\mathbf{x}}^\dagger d_{\mathbf{x}}^\dagger d_{\mathbf{x}} c_{\mathbf{x}} \tag{3}$$

where $J_p^{\mathbf{x}\mathbf{x}'} = J_c^{\mathbf{x}\mathbf{x}'}$, $J_h^{\mathbf{x}\mathbf{x}'} = -J_v^{\mathbf{x}\mathbf{x}'}$ are now the hopping rates of conduction band particles and holes respectively, and U is the strength of the particle-hole attraction. for conduction band atoms and valence band holes, respectively. The attractive interaction may give rise to bound states of conduction band atoms and valence band holes, i.e., ALEs. Although we do not consider this case here, note that $U < 0$ would give rise to repulsively bound excitons, in the same sense as repusively bound atom pairs, which were recently observed experimentally [17] (These would consist of bound pairs where the bound state is higher in energy than the continuum of scattering states, instead of the stable bound states where the bound state has a lower energy than the scattering continuum). In the case of excitons confined to move in 1D, we use the notation $J_p = J_p^{\mathbf{x}\mathbf{x}'}$ and $J_h = J_h^{\mathbf{x}\mathbf{x}'}$. In the setup we consider, we will have $J_h < 0$ and $J_p < 0$.

2.1. The single ALE

In order to obtain the wavefunction for a single ALE, we make an ansatz for the exciton creation operator:

$$\hat{A}^\dagger|v\rangle = \sum_{\mathbf{x}\mathbf{y}} \phi_{\mathbf{x},\mathbf{y}} c_{\mathbf{x}}^\dagger d_{\mathbf{y}}^\dagger |v\rangle, \tag{4}$$

where $|v\rangle$ is the particle-hole vacuum, and $\phi_{\mathbf{x},\mathbf{y}}$ is determined from solution of the eigenvalue equation $H\hat{A}^\dagger|v\rangle = E\hat{A}^\dagger|v\rangle$. We will now investigate the form of $\phi_{x,y}$ for the case of excitons confined in 1D, a result which can also be straightforwardly generalised to 2D or 3D [17, 38].

We can obtain a simple analytical solution that has the same form either for the case $J_p = J_h$, or the case of strongly imbalanced hopping rates, $|J_p| \gg |J_h|$. In the first case, introducing Center-of-mass (COM) and relative coordinates $R = (x+y)/2$, $r = x - y$ gives rise to the product ansatz

$$\phi_{x,y} = \exp\left[\mathrm{i}K(x+y)/2\right] \rho_{x-y}, \tag{5}$$

which solves the eigenvalue equation exactly. The COM quasimomentum $K \in [-\pi/a, \pi/a]$ is factored out, and we are left with equations for the relative wavefunction ρ_r:

$$-J(\rho_{r+1} + \rho_{r-1}) - U\delta_{r0}\rho_r = E\rho_r. \tag{6}$$

Here $J \equiv J_K = 2J_p \cos(Ka/2)$ is the effective hopping rate in relative coordinates and δ_{r0} the Kronecker-delta. Note that the relative wavefunction ρ_r still depends on the centre-of-mass quasimomentum K.

The parameters encountered in an experiment for the suggested implementations of ALEs will typically fulfill $|J_h|/|J_p| \ll 1$, so that holes will appear much heavier than the conduction band atoms. We can make the approximation that the centre of mass is approximately located at the position of the hole, and obtain in this sense a Born-Oppenheimer wavefunction for the single exciton,

$$\phi_{x,y} = C(y)\rho_{x-y}, \tag{7}$$

where $C(y)$ is the wavefunction for the hole. This leads to 6, but now with $J \equiv J_p$.

Eq. 6 can be solved exactly either by direct solution of the difference equation in 1D using a standard exponential ansatz, or using Green's function methods (see Appendix A). For the case of $J_p = J_h$, It yields a single bound state solution for each value of the COM quasimomentum K, ‡, and a continuum of solutions describing unbound states, illustrated in figure 2a. The continuum solutions correspond to scattering states, whilst the bound state solution appears as a Bloch band for the composite object, i.e., the ALE. The wavefunction ρ_r for the bound state solution is given by

$$\rho_r = C\nu^{-|r/a|}, \quad \nu = \frac{-E - \sqrt{(E+2J)(E-2J)}}{2J} \tag{8}$$

$$E = -\sqrt{U^2 + (2J)^2} \tag{9}$$

where C is the normalisation constant and $E < 0$ the energy of the bound state solution. This is depicted in figure 2b. As $U/|J|$ increases, the ALE becomes more tightly bound, and ρ_r decays more rapidly. For $J > 0$, the phase of the wavefunction is constant (given by the phase of C), whereas for $J < 0$, the sign of the ρ_r will oscillate between neighbouring sites.

2.2. Tightly Bound ALEs

In the tightly bound limit, $|J_p|, |J_h| \ll U$, we can interpret ALEs as effective hard-core bosons with creation operators $b_x^\dagger = c_x^\dagger d_x^\dagger$ [39]. The effective Hamiltonian is given by

$$H_{HC} = -J_{\text{eff}} \sum_{\langle ij \rangle} b_i^\dagger b_j + V_{\text{eff}} \sum_{\langle ij \rangle} \hat{n}_i \hat{n}_j, \tag{10}$$

where $\hat{n}_i = b_i^\dagger b_j$. The effective exciton hopping rate J_{eff} can be calculated in degenerate second-order perturbation theory [39], and the dimension-independent result is $J_{\text{eff}} = 2J_pJ_h/U$. A weak nearest-neighbour repulsion also appears in second-order perturbation theory, with $V_{\text{eff}} = (J_p^2 + J_h^2)/U$ again independent of dimensionality [15, 40]. Note that in this limit, where the atoms are treated as hard-core bosons, this form for the interaction precludes the formation of bound states (i.e., bi-excitons).

‡ Note that whilst bound states exist in 1D for any positive value of U, if these equations are solved in 3D, then a bound state only appears above a critical value for the interaction strength $(U/|J)_{crit} \approx 3.95$.

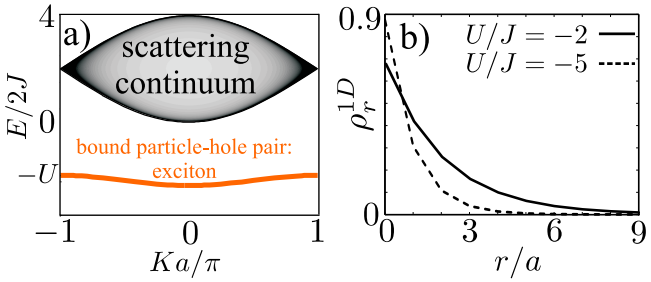


Figure 2. (a) Energy eigenvalues for a single particle and a single hole on a 1D lattice plotted as a function of COM quasimomentum, as found from solution of (6), with $J \equiv J_K$ (see text). The lower curve represents the Bloch Band of a single bound atom-hole pair, the ALE. The upper portion of the spectrum is the scattering continuum of the unbound atom and hole, where the shading corresponds to the density of states (darker shading for higher density of states). (b) Bound-state relative wavefunctions at different binding energies E_b/J, valid both for $J_h = J_p$ ($J \equiv J_K$, see text), and also in the limit $|J_h| \ll |J_p| \equiv J$. Weakly bound states have an appreciable range over 10 or 20 sites. This falls substantially for moderately bound states (dashed line).

2.3. Interaction of ALEs: The Born-Oppenheimer approximation

In the typical experimental situation, where $J_p \gg J_h$, we can treat ALE-ALE interactions in a Born-Oppenheimer (BO) approximation, and observe longer range interactions mediated by the faster tunnelling conduction band atoms. We find it convenient to derive the results in this limit for the general case in D dimensions, although we will again primarily apply them in the 1D case.

The basic idea is that we initially assume the holes to be essentially static (i.e. $J_h \approx 0$) at a given set of positions $\underline{\mathbf{R}} = \{\mathbf{R}_1, \mathbf{R}_2, \ldots, \mathbf{R}_N\}$. The conduction band atoms then move with hopping rate J_p in the static potential given by the holes, and have coordinates denoted $\underline{\mathbf{r}} = \{\mathbf{r}_1, \mathbf{r}_2, \ldots, \mathbf{r}_N\}$. In this sense, we begin by decomposing the full Hamiltonian into two parts, one describing slow-moving holes (H_h) and one particle motion and particle-hole interaction H_{BO}. In first quantisation we obtain

$$\begin{aligned} H &= H_h + H_{BO} \\ H_h &= -\sum_{n=1}^{N} J_h \widetilde{\Delta}_{\mathbf{R}_n} \qquad (11) \\ H_{BO} &= \sum_{n=1}^{N} \left[-J_p \widetilde{\Delta}_{\mathbf{r}_n} - U \sum_{n'=1}^{N} \delta_{\mathbf{r}_n \mathbf{R}_{n'}} \right], \qquad (12) \end{aligned}$$

where the operator

$$\tilde{\Delta}_{\mathbf{x}} \Psi(\mathbf{x}, \mathbf{y}) = \sum_{d=1}^{D} \left[\Psi(\mathbf{x}+\mathbf{e}_d, \mathbf{y}) + \Psi(\mathbf{x}-\mathbf{e}_d, \mathbf{y}) - 2\Psi(\mathbf{x}, \mathbf{y}) \right] \qquad (13)$$

denotes a discrete lattice Laplacian on a cubic lattice with unit vectors $\mathbf{e}_d$ in D dimensions. Note that we have shifted the zero of energy by $N(2J_p + 2J_h)$ for convenience in writing the discrete Laplacian.

We write the full time-dependent many-body wavefunction of the ALEs as

$$\psi(\underline{\mathbf{r}}, \underline{\mathbf{R}}, t) = \sum_{\alpha} C_\alpha(\underline{\mathbf{R}}, t) \phi_\alpha(\underline{\mathbf{r}}; \underline{\mathbf{R}}). \qquad (14)$$

Here, the functions $\phi_\alpha(\underline{\mathbf{r}};\underline{\mathbf{R}})$ are solutions of the Schrödinger equation for motion of the particles in the static potential provided by the holes,

$$H_{BO}[\underline{\mathbf{R}}]\phi_\alpha(\underline{\mathbf{r}};\underline{\mathbf{R}}) = E_{\alpha;BO}[\underline{\mathbf{R}}]\phi_\alpha(\underline{\mathbf{r}};\underline{\mathbf{R}}). \tag{15}$$

where $\underline{\mathbf{R}}$ are considered parameters.

In order to obtain an equation for the functions $C_\alpha(\underline{\mathbf{R}},t)$, we apply the full Hamiltonian to (14), multiply with $\phi^*_\beta(\underline{\mathbf{r}};\underline{\mathbf{R}})$ and trace over the $\underline{\mathbf{r}}$s:

$$\begin{aligned}\mathrm{i}\partial_t C_\alpha(\underline{\mathbf{R}},t) = &\left[-J_h\sum_{n=1}^{N}\widetilde{\Delta}_{\mathbf{R}_n} + E_{\alpha;BO}[\underline{\mathbf{R}}]\right]C_\alpha(\underline{\mathbf{R}},t)\\ &-J_h\sum_{\beta}\sum_{n=1}^{N}\sum_{d=1}^{D}\sum_{\epsilon=\pm}C_\beta(\underline{\mathbf{R}}+\epsilon\underline{\mathbf{e}_d}^n,t)\left\{\sum_{\underline{\mathbf{r}}}\phi^*_\alpha(\underline{\mathbf{r}};\underline{\mathbf{R}})\left[\phi_\beta(\underline{\mathbf{r}};\underline{\mathbf{R}}+\epsilon\underline{\mathbf{e}_d}^n)-\phi_\beta(\underline{\mathbf{r}};\underline{\mathbf{R}})\right]\right\}\end{aligned} \tag{16}$$

where $\underline{\mathbf{e}_d}^n = \{0,\ldots,0,\mathbf{e}_d,0,\ldots,0\}$ represent the D different unit vectors on the lattice for the n-th hole coordinate. This describes the dynamics of our system as a multi-channel problem, with each α denoting a particular channel, corresponding to an eigenstate found from (15). The first term describes the hole dynamics for a single channel, with the holes moving in the effective potential $E_{\alpha;BO}[\underline{\mathbf{R}}]$. The second term provides coupling between the channels, and has the general form of another discrete Laplacian acting on $C_\beta(\underline{\mathbf{R}},t)$, where each hopping process now carries $\underline{\mathbf{R}}$- and α-dependent coefficients.

If the terms corresponding to coupling between the channels are small, then we can reduce the wavefunction expansion, (14) to a single value of α. This we will do for the lowest energy solution to (15), $\phi_\gamma(\underline{\mathbf{r}};\underline{\mathbf{R}})$, which corresponds to N bound ALES. We can then interpret the corresponding function $C_\gamma(\underline{\mathbf{R}},t)$ as the wavefunctions of the composite ALEs, moving in a potential obtained from the wavefunctions $\phi_\gamma(\underline{\mathbf{r}};\underline{\mathbf{R}})$. This interpretation amounts to an adiabatic approximation in the ratio of the coupling terms in (16) with $\gamma \neq \beta$ and the energy separation $|E_{\gamma;BO}[\underline{\mathbf{R}}] - E_{\beta;BO}[\underline{\mathbf{R}}]|$ of the modes γ,β. This approximation will be satisfied if the ratio $J_h/J_p \ll 1$, as the separation of the modes is at least as large as J_p, see figure 3b for an illustration. However, this approximation can have a much larger range of validity in practice, if the energy difference $|E_{\gamma;BO}[\underline{\mathbf{R}}] - E_{\beta;BO}[\underline{\mathbf{R}}]|$ is greater than or equal to the binding energy of a single ALE. For example, this approximation is clearly also valid provided $J_h \ll U$, c.f. figure 3b.

The diagonal terms $\alpha = \beta$ in the second rhs.-term of (16) give an effective renormalisation of the hopping rate J_h that appears in the kinetic energy term in the first line of the same equation. This assumes that the coefficients given by the trace over $\underline{\mathbf{r}}$ are approximately equal for all $\underline{\mathbf{R}}$, which we have confirmed by evaluation of the corresponding terms from exact calculations in 1D. We find maximum variation of the coefficients of the order of 15% even when two holes are very close (within $\sim$ 2 sites), whilst for a more dilute gas, this approximation becomes even better. The renormalised kinetic energy can be interpreted as the kinetic energy term of the composite exciton, and in the tightly bound limit, $|J_p|, |J_h| \ll U$, reduces to the values found in sec. 2.2.

The solution of 15 is simplified in our case because the particles are non-interacting fermions, and thus the problem reduces to finding the solutions for a particle on a lattice with N impurities. This is detailed in Appendix B. We assume throughout

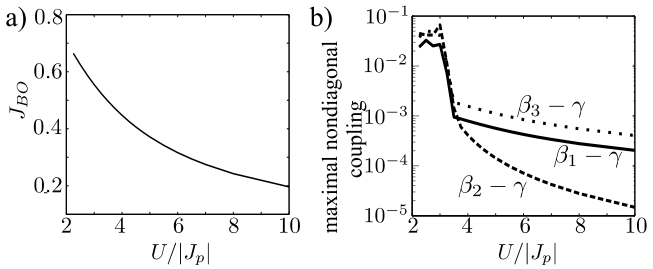


Figure 3. Diagonal and nondiagonal contributions of the last term of (16) for $N = 3$ and $J_h/J_p = 0.1$ for a 60-site lattice. (a) J_{BO} plotted as a function of $U/|J_p|$, computed from the diagonal elements. As ALEs become more tightly bound, the result approaches that obtained from perturbation theory, $J_{eff} = 2J_pJ_h/U$. (b) Maximal effective coupling between the lowest channel γ and the first three excited channels β_1, β_2, β_3 arising from the off-diagonal elements, $\max_{\underline{R},n}\{|J_p\sum_{\underline{r}}\phi^*_\gamma(\underline{r};\underline{R})\phi_\beta(\underline{r};\underline{R}\pm\underline{e}^n)/(E_{\beta;BO}[\underline{R}\pm\underline{e}^n]-E_{\gamma;BO}[\underline{R}])|\}$. Even for low $U/|J_p|$, nonadiabatic coupling will always add just small perturbative corrections, provided $|J_h/J_p|$ is sufficiently small.

that the N impurities are sufficiently separated from each other that N bound states exist. The critical separation at which bound states occur is dependent upon $U/|J_p|$ and the number of particles. For $N = 2$ bound states exist even when holes are on neighbouring sites provided $U/|J_p| \gtrsim 2$.

For $N = 2$, The single-particle bound states are then the symmetric and antisymmetric superpositions $\rho_\pm$ (B.3) of two exponentially decaying bound states, centred at $\mathbf{R}_1$ and $\mathbf{R}_2$. These take the same form as the single ALE wavefunction, (8), but now with different energy E that depends on the separation $R = |\mathbf{R}_1 - \mathbf{R}_2|$. The lowest-energy two-atom wavefunction $\phi(\mathbf{r}_1, \mathbf{r}_2; \mathbf{R}_1, \mathbf{R}_2)$ is then obtained from the Slater-determinant of $\rho_\pm$. In principle, the choice of overall phase of these solutions can be made differently for different $\mathbf{R}_1, \mathbf{R}_2$. Without loss of generality we can choose each $\phi(\mathbf{r}_1, \mathbf{r}_2; \mathbf{R}_1, \mathbf{R}_2)$ to be real, leaving us with a choice as to whether $\phi(\mathbf{r}_1, \mathbf{r}_2; \mathbf{R}_1, \mathbf{R}_2)$ should be symmetric or antisymmetric under exchange of hole coordinates $\mathbf{R}_1$ and $\mathbf{R}_2$. However, in order to minimise the non-adiabatic terms in (16), we are required to choose these to be antisymmetric under exchange of $\mathbf{R}_1$ and $\mathbf{R}_2$, in addition to the requirement of antisymmetry under exchange of particle coordinates $\mathbf{r}_1$ and $\mathbf{r}_2$. It then follows that in order to ensure the correct antisymmetry for exchange of hole coordinates $\mathbf{R}_i$ in the total wavefunction $\psi(\underline{\mathbf{r}}, \underline{\mathbf{R}}, t)$, [(14)], that $C_\gamma(\mathbf{R}_1, \mathbf{R}_2, t)$ must be *symmetric* under exchange of coordinates $\mathbf{R}_i$. In the limit where the BO approximation is valid, we can then interpret the coordinates $\mathbf{R}_i$ as approximate centre of mass coordinates for the ALEs, which behave under this approximation as composite bosons.

The lowest values of the potential $E_{\gamma;BO}[R_1, R_2]$ in 1D are shown for various values of $U/|J_p|$ in figure 4, where the zero of energy is chosen so that $E_{\alpha;BO}[R_1, R_2] \to 0$ as $R = |R_1 - R_2| \to \infty$. For large $U/|J_p|$, interactions are very short-ranged, reducing to the values found in section 2.2. As $U/|J_p|$ is decreased, the increase in mobility of the conduction band atoms leads first to increased interaction strength, and then as $U/|J_p|$ is further decreased, to longer-range interactions. These are shown in the figure around the parameter values where they become significant over 2-3 sites, which is approximately between $U/|J_p| = 2$ and $U/|J_p| = 3$. For finite J_h these interactions will be important as long as the energy of the COM-motion is not much larger than

the interaction energy.

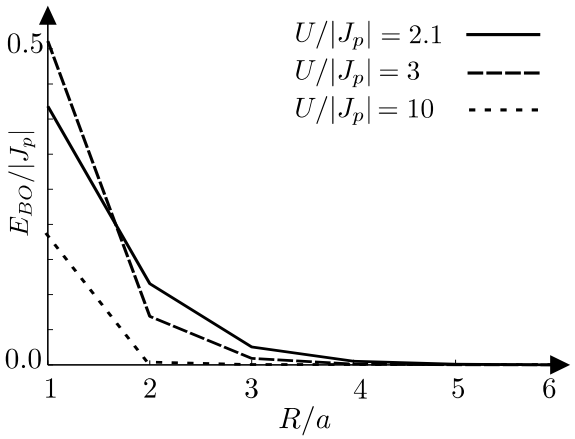


Figure 4. Born-Oppenheimer curves for the interaction between two ALEs as a function of separation R, for different values of $U/|J_p|$. For $U/|J_p| \approx 2-3$, longer-range interactions are significant. For tightly bound excitons however, the Born-Oppenheimer approximation recovers the perturbative limit, in which only nearest-neighbour interactions are appreciable. The zero of energy is chosen so that all curves are to zero in the limit $R/a \gg 1$.

For $N > 2$, we can always decompose the potential $E_{\alpha;BO}[\underline{\mathbf{R}}]$ into a sum over contributions from different numbers of particles.

For example, for $N = 3$ we can take the two-body potential $E^{(2)}_{\alpha;BO}[\mathbf{R}_1, \mathbf{R}_2]$ found for two particles (when the third is an infinite distance from the first two), and define the 3-body interaction $E^{(3)}_{\alpha;BO}[\mathbf{R}_1, \mathbf{R}_2, \mathbf{R}_3]$ such that

$$E_{\alpha;BO}[\underline{\mathbf{R}}] = E^{(3)}_{\alpha;BO}[\mathbf{R}_1, \mathbf{R}_2, \mathbf{R}_3] + \sum_{i<j} E^{(2)}_{\alpha;BO}[\mathbf{R}_i, \mathbf{R}_j]. \tag{17}$$

By solving (15) for $N = 2$ and $N = 3$ we can thus assess the importance of genuine three body interactions. Typical results for the 1D case, in which we are primarily interested, are ploted in figure 5. They show two typical solutions for $E^{(3)}_{\alpha;BO}[0, R_2, R_3]$, and we see that only for low $U/|J_p|$ there are any appreciable three-body interactions, even at small distances. The same will be true for larger N provided that the density remains sufficiently small. Thus, for cold ALEs at sufficiently small densities, the BO-potentials in (16) can be decomposed into a sum of two-hole interactions,

$$E_{\alpha;BO}[\underline{\mathbf{R}}] \approx \sum_{i<j} E^{(2)}_{\alpha;BO}[\mathbf{R}_i, \mathbf{R}_j]. \tag{18}$$

There are two cases where the symmetry properties of the two particle wavefunction also transfer to the N-body case. The first is the limit of two-body collisions, where the only significant interactions are those between each particle and its nearest neighbour,

$$E_{\alpha;BO}[\underline{\mathbf{R}}] \approx \frac{1}{2} \sum_i \max_j E^{(2)}_{\alpha;BO}[\mathbf{R}_i, \mathbf{R}_j]. \tag{19}$$

In this limit, we can construct $\phi_\alpha(\underline{\mathbf{r}}; \underline{\mathbf{R}})$ from a Slater determinant of single particle bound states at single holes or combinations of two holes, and the arguments presented

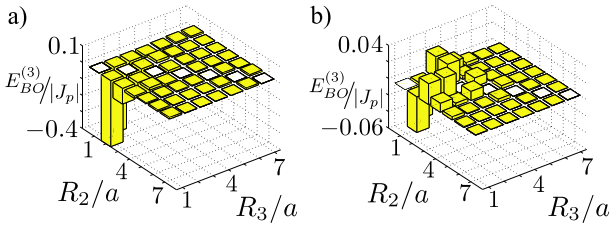


Figure 5. Three-body interactions between ALEs $E^{(3)}_{\alpha;BO}[0, R_2, R_3]$ computed in the Born-Oppenheimer approximation curves for (a) $U/|J_p| = 2.1$ and (b) $U/|J_p| = 3$. These results should be compared to the two-body interactions plotted in figure 4. Even when the three ALEs are close together, the three-body interactions are dominated by two-body interactions, with three-body interactions becoming extremely small for $U/|J_p| \gtrsim 3$. This is still the case near the limit $U/|J_p| \sim 2$, at which limit one bound state disappears for the case of ALEs existing on neighbouring lattice sites.

for the two-particle case will generalise. The other case is that in which the holes are evenly spaced. There, the correct wavefunction is again the Slater determinant of single particle bound states centred at each hole, irrespective of the separation provided that the N bound states exist. This problem can be seen analogously to that of a periodic potential in free space, with the single particle bound states at each hole playing the role of Wannier functions for this periodic structure. In each of these cases, the optimal choice for the Born-Oppenheimer approximation is that $\phi_\alpha(\underline{\mathbf{r}}; \underline{\mathbf{R}})$ is antisymmetric under exchange of hole or particle coordinates, and it follows that the wavefunction $C_\gamma(R_1, \ldots, R_N)$ will be symmetric under exchange of coordinates $\mathbf{R}_i$, as discussed above for the $N = 2$ case.

In either of these regimes, we then can write an effective Hamiltonian for the ALEs as composite bosons with creation operators b_x, which in 1D takes the form

$$H_{HC} = -J_{\mathrm{BO}} \sum_{\langle ij \rangle} b_i^\dagger b_j + \sum_{\langle i,l \rangle} V_l \hat{n}_i \hat{n}_{i+l}, \quad V_l = E^{(2)}_{\alpha;BO}[R_0, R_l], \tag{20}$$

$\hat{n}_i = b_i^\dagger b_j$, and J_{BO} is the renormalised effective hopping given by the first and last terms in (16). It can be approximately calculated from the solution to the single impurity problem ($N = 1$), $\tilde{\phi}_\gamma(r_1 - R_1)$, as

$$J_{\mathrm{BO}} \approx J_h \sum_{r_1} \tilde{\phi}^*_\gamma(r_1 - R_1)\tilde{\phi}_\gamma(r_1 - R_1 + 1). \tag{21}$$

In figure 3a, J_{BO} is plotted.

In this section we have effectively shown how imbalance in the hopping rates can enhance the strength and range of interactions between ALEs. This will lead to the stabilization of diagonal order, i.e. crystaline order away from half-filling, which is discussed in detail in Sec. 3.1. Note that this limit is extremely relevant for ALEs, where J_p will typically be an order of magnitude larger than J_h, and where the lifetime of an ALE is sufficiently long for longer range interactions to form a crystaline structure.

2.4. Interaction of ALEs: Numerical results

Beyond the tight-binding and Born-Oppenheimer cases, we have also performed small-scale exact diagonalizations for two interacting excitons in 1D, using parameters

ranging from $U/|J| = 1$ to $U/|J| = 25$ on up to 22 lattice sites. Strong imbalances in the hopping rates of holes and particles were considered as well, ranging from $J_h/J_p = 1$ to $J_h/J_p = 1/40$. All these calculations show only effective repulsion between the two excitons and a complete absence of bound states of four particles. A typical result is depicted in figure 6, where the scattering continuum and the dispersion relation of the anti-bound state resulting from weak repulsion can be clearly distinguished.

In all cases in 1D that we have analyzed, both analytically and numerically, we only find repulsive interactions, and thus no bound states. With increasing spatial dimensionality, it becomes generally more unlikely for bound states to form in scattering problems, and thus we also expect that this result will hold for arbitrary values of $|J_h|/U, |J_p|/U$ in 2D and 3D.

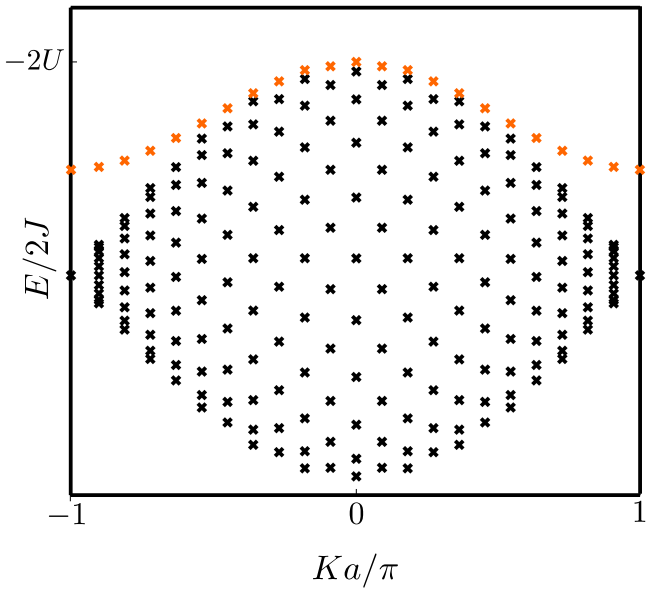


Figure 6. Discrete energy eigenvalues for two interacting excitons on 22 lattice sites, plotted as a function of quasimomentum. Black crosses correspond to scattering states. Orange crosses form the dispersion relation of a repulsively bound state resulting from weak exciton-exciton repulsion.

3. Many ALEs at low temperatures - exciton condensates and crystals

Much fundamental interest in semiconductor excitons has stemmed from their predicted ability to undergo condensation in 3D or to form quasicondensates in 1D. Due to their isolation from the environment, ALEs present an opportunity to investigate exciton condensation in a clean and highly controllable environment. In addition, the long lifetimes of ALEs, combined with long range interactions that are found in the case of unbalanced hopping give rise to other potentially interesting phases, especially an ALE crystal.

3.1. The ALE condensate

Due to the effective bosonic nature of ALEs, we expect them to form a condensate characterised by off-diagonal Long-Range Order (ODLRO) at sufficiently low temperatures, in analogy to semiconductor excitons [2]. This should be true irrespective of whether the excitons are strongly or weakly bound.

3.1.1. Continuum approach The mean-field approximation normally made for semiconductor excitons is a continuum model, and can be generalised to the lattice in order to obtain a description of the ALE groundstate at zero-temperature. In the continuum limit we write the Hamiltonian as

$$H = \sum_{\mathbf{k}} \left[E^p_{\mathbf{k}} c^\dagger_{\mathbf{k}} c_{\mathbf{k}} + E^h_{\mathbf{k}} d^\dagger_{\mathbf{k}} d_{\mathbf{k}} \right] + \sum_{\mathbf{klq}} \left[\frac{1}{2} V^p_{\mathbf{q}} c^\dagger_{\mathbf{k+q}} c^\dagger_{\mathbf{l-q}} c_{\mathbf{l}} c_{\mathbf{k}} + \frac{1}{2} V^h_{\mathbf{q}} d^\dagger_{\mathbf{k+q}} d^\dagger_{\mathbf{l-q}} d_{\mathbf{l}} d_{\mathbf{k}} + V_{\mathbf{q}} c^\dagger_{\mathbf{k+q}} d^\dagger_{\mathbf{l-q}} d_{\mathbf{l}} c_{\mathbf{k}} \right], \tag{22}$$

where $E^p_{\mathbf{k}}$ and $E^h_{\mathbf{k}}$ are the dispersion relations for particles and holes respectively, and $V^p_{\mathbf{q}}$, $V^h_{\mathbf{q}}$ and $V_{\mathbf{q}}$ denote the effective interaction potentials for particle-particle, hole-hole, and particle-hole interactions, respectively. The exciton creation operator can then be written as

$$\hat{A}^\dagger_\alpha |0\rangle = \sum_{\mathbf{k},\mathbf{k}'} A_\alpha(\mathbf{k},\mathbf{k}') c^\dagger_{\mathbf{k}} d^\dagger_{\mathbf{k}'} |0\rangle, \tag{23}$$

where the index α will specify the quantum numbers for the exciton. The key observation is that the single-exciton state of lowest energy will have the lowest possible bound-state level $n = 0$, and COM-momentum $\mathbf{K} = \mathbf{w}$. Here, $\mathbf{w}$ denotes the difference in position between the maximum of the valence band and the minimum of the conduction band. It can either be $\mathbf{0}$ or half a reciprocal lattice vector. If $\mathbf{w} = \mathbf{0}$ (as was the case for the 1D ALEs in the previous section) the system has a *direct band gap*. Whereas for $\mathbf{w} \neq \mathbf{0}$ it has an *indirect band gap* (the 2D and 3D realization of ALEs are of this form).

In the following, the dispersion relations of the valencce band, is shifted by $-\mathbf{w}$. Then the single exciton operator of lowest energy with $\alpha = (\mathbf{w}, 0)$ has the form $\hat{A}^\dagger_{0,0}|0\rangle = \sum_{\mathbf{k}} A(\mathbf{k}) c^\dagger_{\mathbf{k}} d^\dagger_{-\mathbf{k}} |0\rangle$ with $A(\mathbf{k}) = A_{0,0}(\mathbf{k}, -\mathbf{k})$. Such a state corresponds to an effective pairing of electron at $\mathbf{k}$ and hole at $\mathbf{w} - \mathbf{k}$ (when the notational shift of the hole-quasimomenta is reversed). The equivalent of this pairing in an approximate many-body groundstate emerges from an ansatz first proposed by Keldysh and Kozlov [1]. There, the ground state of the system is assumed to be a coherent state for this single-exciton operator $\hat{A}^\dagger_{0,0}$,

$$\mathcal{D}|0\rangle = \exp\left[\sqrt{n_{ex}} (\hat{A}^\dagger_{0,0} - \hat{A}_{0,0}) \right] |0\rangle = \prod_p (u_{\mathbf{k}} + v_{\mathbf{k}} c^\dagger_{\mathbf{k}} d^\dagger_{-\mathbf{k}}) |0\rangle, \tag{24}$$

$$u_{\mathbf{k}} = \cos(\sqrt{n_{ex}} A(\mathbf{k})) \quad v_{\mathbf{k}} = \sin(\sqrt{n_{ex}} A(\mathbf{k})). \tag{25}$$

The resultant state has the same structure as the BCS ground state of weakly correlated electrons in a superconductor. At finite density the coefficients $A(\mathbf{k})$ in (24) and (25) are no longer the single-exciton ground state wavefunction. Instead, the coefficients $u_{\mathbf{k}}$ and $v_{\mathbf{k}}$ have to be determined in a self-consistent manner

(see Appendix C) for background). In mean-field theory and using the constraint of fixed density these are found to be

$$\Delta^P_{\mathbf{k}} = -\sum_{\mathbf{l}} V_{\mathbf{l}-\mathbf{k}} \frac{\Delta^P_{\mathbf{l}}}{E^P_{\mathbf{l}}}, \quad n_{ex} = \frac{1}{2}\sum_{\mathbf{l}} \left(1 - \frac{\xi_{\mathbf{l}}}{E^P_{\mathbf{l}}}\right) \tag{26}$$

where

$$\xi_{\mathbf{k}} = E^c_{\mathbf{k}} + E^h_{\mathbf{k}} + 2\sum_{\mathbf{l}} \Sigma_{\mathbf{l}-\mathbf{k}} v^2_{\mathbf{l}} \tag{27}$$

$$\Sigma_{\mathbf{k}} = V_0 + \frac{1}{2}\left(V^p_0 + V^h_0 - V^p_{\mathbf{k}} - V^h_{\mathbf{k}}\right) \tag{28}$$

$$\Delta^P_{\mathbf{k}} = -\sum_{\mathbf{l}} V_{\mathbf{l}-\mathbf{k}} u_{\mathbf{l}} v_{\mathbf{l}} \tag{29}$$

$$E^P_{\mathbf{k}} = \sqrt{\xi^2_{\mathbf{k}} + (2\Delta^P_{\mathbf{k}})^2}. \tag{30}$$

In this regime the Hamiltonian (22) can be diagonalised with new fermionic quasiparticle and quasihole operators $C^\dagger_{\mathbf{k}}$ and $D^\dagger_{\mathbf{k}}$ [see (C.1)] to yield

$$H_{MF} = \sum_{\mathbf{k}} \left(E^{(1)}_{\mathbf{k}} C^\dagger_{\mathbf{k}} C_{\mathbf{k}} + E^{(2)}_{\mathbf{k}} D^\dagger_{\mathbf{k}} D_{\mathbf{k}}\right), \tag{31}$$

with the expressions for the new quasiparticle dispersion relations $E^{(1)}_{\mathbf{k}}$, $E^{(2)}_{\mathbf{k}}$ given in Appendix C, (C.6), (C.7).

As a consequence of this ansatz for the groundstate, the lowest energy solution $(\mathbf{k}, n) = (0, 0)$ of the single exciton can be recovered from the above mean-field equations in the limit of vanishing density $n_{ex} \to 0$ [41].

The condensate thus exhibits off-diagonal long-range order, with the associated dissipationless transport properties. For excitons, however, these involve only dissipation-free transport of excitation energy and momentum, not of mass or charge transfer.

3.1.2. ALE condensate on a lattice We can adapt Hamiltonian (22) - and the mean-field results derived from it - directly to the case of ALEs, where $\mathbf{k}$ now denotes lattice quasimomenta in the first Brillouin-zone (B.Z.) instead of momenta in the continuum case, and we set $V^p_{\mathbf{q}} = 0$, $V^h_{\mathbf{q}} = 0$, $V_{\mathbf{q}} = -U$. Using Hamiltonian (3) and applying (26) - (30), the condensate at zero temperature can be approximated by a BCS-type groundstate

$$|\Psi\rangle = \prod_{\mathbf{k}} (u_{\mathbf{k}} + v_{\mathbf{k}} c^\dagger_{\mathbf{k}} d^\dagger_{-\mathbf{k}})|0\rangle \tag{32}$$

where $u_{\mathbf{k}}$ and $v_{\mathbf{k}}$ must obey the gap-equation and the density constraint [41, 42, 43]:

$$U^{-1} = a^D \int_{B.Z.} \frac{\mathrm{d}^D k}{(2\pi)^D} \frac{1}{E^P_{\mathbf{k}}}, \quad n_{ex} = \frac{a^D}{2} \int_{B.Z.} \frac{\mathrm{d}^D k}{(2\pi)^D} \left(1 - \frac{\xi_{\mathbf{k}}}{E^P_{\mathbf{k}}}\right) \tag{33}$$

where

$$\xi_{\mathbf{k}} = -\sum_{d=1}^{3} (J^d_p + J_h)\cos(k_d a) - \mu_{ex} + 2U n_{ex}, \tag{34}$$

$$E^P_{\mathbf{k}} = \sqrt{\xi^2_{\mathbf{k}} + (2\Delta^P)^2}, \tag{35}$$

and J_p^d denotes the hopping rates of conduction band atom in the d-th direction. As the conduction band is assumed anisotropic (see Sec. 2), $J_p^1 \neq J_p^2, J_p^3$ will hold generally, with $J_p^1 < 0$, $J_p^2, J_p^3 > 0$ [27]. Consequently, the conduction band has its minima around $(\pm\pi/a, 0, 0)$, and thus $\mathbf{w} = (0, \pi/a, \pi/a)$. Contrary to the situation in 1D, the system thus has an indirect gap, and at zero temperature the ALEs condense into a motional state with nonzero quasimomentum.

Evaluating (C.6) and (C.7) for the given model of ALEs yields the dispersion-relations of the new quasiparticles and quasiholes respectively:

$$E_{\mathbf{k}}^{(1)} = \frac{1}{2}\left(E_{\mathbf{k}}^p - E_{\mathbf{k}}^h + E_{\mathbf{k}}^P\right), \quad E_{\mathbf{k}}^{(2)} = \frac{1}{2}\left(E_{\mathbf{k}}^h - E_{\mathbf{k}}^p + E_{\mathbf{k}}^P\right) \tag{36}$$

where

$$E_{\mathbf{k}}^p = -2\sum_{d=1}^{D} J_p^d \cos(k_d a), \quad E_{\mathbf{k}}^h = -2\sum_{d=1}^{D} J_h \cos(k_d a). \tag{37}$$

For two-band implementation of ALEs considered here, where $J_p^d \neq J_h$ in 2D and 3D, the quasiparticle dispersion relations are different, $E_{\mathbf{k}}^{(1)} \neq E_{\mathbf{k}}^{(2)}$. Thus they exhibit minima at different points in the Brillouin zone.

As shown in [41, 42], this BCS-formalism can interpolate between the weak-coupling $U \ll |J_p^d|, |J_h|$ and strong-coupling $U \gg |J_p^d|, |J_h|$ regime, provided the Hartree-Fock corrections to the chemical potential are included. For strong coupling it also becomes exact in the low-density regime ($n_{ex} \approx 0$) and provides a good qualitative description of the groundstate for increasing density up to the case of maximal filling, $n_{ex} \approx \frac{1}{2}$.

In Sec. 4 we will discuss measurements that can be made on exciton condensates, including determination of the condensate fraction and pairing correlations.

3.2. The ALE crystal in 1D

The long range repulsive interactions that we found for large hopping imbalances $J_p \gg J_h$ in Sec. 2.2 suggest the possibility of forming an ALE crystal for densities away from half filling, $n_{ex} \neq \frac{1}{2}$. This situation is directly related to recent research on Fermi Hubbard models with imbalanced hopping rates for the two species [40, 44].

The results of the Born-Oppenheimer approximation in Sec. 2.3 suggest that the effective interactions have maximal range and strength for loosely bound ALEs at $U/|J_p| \approx 2$ - 3 for large hopping imbalances. For these parameters, naive inspection of figure 4 suggests that interaction effects will favour Diagonal Long Rangle order (DLRO), i.e., a crystal, and suppress pairing maximally from $n_{ex} \approx \frac{1}{3}$ upward, provided that the kinetic energy of the ALEs is sufficiently small. We investigate the possibility of such a crystal using imaginary time evolution on matrix product states (with a time-depndent DMRG algorithm) [45, 46, 47, 48] to compute the groundstate Hamiltonian (3) at different densities. From the numerically calculated groundstates, we obtained density-density- and pairing correlations for four different densities, with $n_{ex} = \frac{15}{96}$ $\frac{23}{96}$, $\frac{30}{96}$ and $\frac{39}{96}$, on a 96-site lattice for different values of $U/|J_p|$ and J_h/J_p.

In bosonised theories [49], the Luttinger parameter K determines the algebraic decay of correlation functions in the thermodynamic limit at large distances (true long-range order of any type being absent in 1D for continuously-valued fields). We expect the pairing correlation function $\langle c_x^\dagger d_x^\dagger d_y c_y\rangle$ to behave as $A_P/|x-y|^{K_P}$, and the density-density-correlation function $(\langle n_x n_y\rangle - \langle n_x\rangle\langle n_y\rangle)$ to behave as $A_{DD}\cos(k_f(x-$

$y))/|x-y|^{K_{DD}}$ for $|x-y| \gg 1$, where $k_f = \pi n_{ex}$ denotes the Fermivector. A_P, A_{DD}, K_P and K_{DD} were determined from fitting to these functions.

Bosonisation predicts $K_{DD} = 1/K_P$ [49]. The validity of bosonization will shift to decreasing wavelengths, however, as J_h/J_p decreases. This results from the increasingly different slopes of the dispersion-relation linearisation around the Fermi-points. Excitations that are still weak - i.e. long-wavelength - for the more mobile conduction-band atoms, will be in the non-linear regime for the slower atomic holes. The validity of bosonization for any finite-size system is thus limited by the length-scale set by the less mobile holes, and we expect our simulation results to exhibit noticeable deviations from bosonization predictions below some value of J_h/J_p.

While we averaged out k_f-oscillations superimposed on the algebraically decaying pairing correlations (c.f. [50]) to obtain reliable fits for K_P, this is more difficult for K_{DD} in the density-density-correlations. As a result, we obtain large deviations from the bosonization prediction $K_{DD} = 1/K_P$ even for $J_p = J_h$, where bosonization is most reliable. Despite this difficulty, we can identify clearly different regimes of behaviour, dependent on the hopping imbalance and ALE density. For illustration, the powers of algebraic decay obtained from the fit are depicted in figure 7 for the pairing correlations, while figure 8 shows representative examples of density-density correlation functions in different parameter regimes. Generally we observe in our results that superfluid order is dominant for equal or moderately imbalanced hopping rates, but becomes more and more suppressed as ALE density and hopping imbalance increase. Complementary, density-density-correlations start decaying slower and become the dominant order. As is to be expected in 1D, this superfluid-to-crystal transition is continuous. Crystaline behaviour is especially pronounced in the region predicted from Born-Oppenheimer calculations, i.e. as $n_{ex} \geq \frac{1}{3}$ and $U/|J_p| = 2 - 3$, where density-density-correlations decay only moderately (figure 8) and ALE-interactions suppress pairing very strongly (figure 7).

For higher dimensions, the subject of crystal formation close to half-filling for general values of $U/|J_p|, U/|J_h|$ has recently been addressed using both numerical DMFT and analytical mean-field analysis [44]. The results are directly applicable to loosely bound ALEs. Both DMFT and standard mean-field calculations show the ALEs to form a superfluid condensate for moderate hopping imbalances, and to phase separate into checkerboard crystal and superfluid below some critical, density-dependent value of J_h/J_p (c.f. figure 1 in [44]). For a parameter regime analogous to the one considered here (large hopping imbalance, loosely bound ALEs) analytical mean-field calculations additionally predict the possibility of pure crystal phase at noncommensurate densities (c.f. figure 2 in [44]). As the DMFT calculations do not yield such a phase, the authors question the validity of this result. Whether ALE-interactions can thus suppress superfluidity at large hopping imbalances sufficiently for the formation of a stable noncommensurate crystal phase in higher spatial dimensions is not fully resolved yet.

As a final comment, note that the Hamiltonian (3) with $J_p \neq J_h$ used here to describe ALEs, has been studied previously in 1D [40] using Luttinger liquid theory. There, the authors showed that increasing hopping imbalance can lower the value K_c, the exponent controlling the algebraic decay of correlation functions. For $|x-y| \gg 1$, density-density (DD) correlations decay as $(\langle n_x n_y\rangle - \langle n_x\rangle\langle n_y\rangle) \sim \cos(k_f(x-y)))/|x-y|^{K_c}$, with $n_x = c_x^\dagger c_x + d_x^\dagger d_x$, whereas pairing-correlations decay as $\langle c_x^\dagger d_x^\dagger d_y c_y\rangle \sim 1/|x-y|^{1/K_c}$ [49]. As J_h/J_p decreases, K_c can decrease below 1. Then crystaline ordering becomes dominant over superfluid ordering, which is dominant for

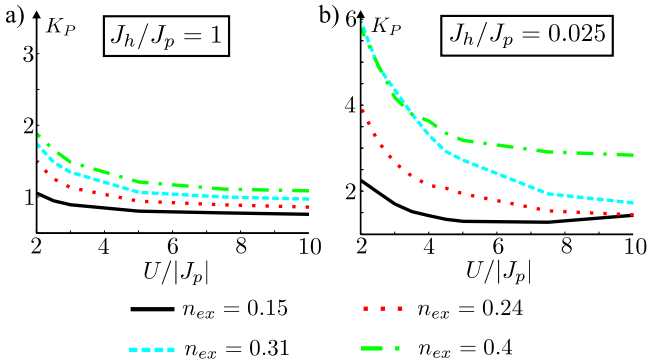


Figure 7. Power of algebraic decay of pairing correlations plotted as a function of $U/|J_p|$ for $J_p/J_h = 1$ and $J_p/J_h = 0.025$, and for four different densities on a 96-site lattice. (a) For $J_h/J_p = 1$, pairing correlations decay moderately faster with increasing density and decreasing $U/|J_p|$. (b) For strong hopping imbalance, pairing correlations decay much faster with decreasing $U/|J_p|$ as ALE-ALE interaction increases in range and magnitude, which become more significant as n_{ex} increases. The decay is especially strong for $n_{ex} \geq 0.3$ in the regime $U/|J_p| \approx 2 - 3$. From the Born-Oppenheimer theory this result is expected, see e.g. figure 4, as for these parameters and $J_h/J_p = 0.025$ the next-nearest-neighbour interactions between ALEs is still dominant over the kinetic energy of the COM-motion of the ALEs. As a result, for $n_{ex} = 0.31$, close to the ideal crystal filling factor $n_{ex} = \frac{1}{3}$, the decay also shows the steepest increase as $U/|J_p|$ decreases. The enhanced next-nearest-neighbour interactions in this region strongly suppress pairing order, and thus for the ALEs crystaline order dominates in this regime.

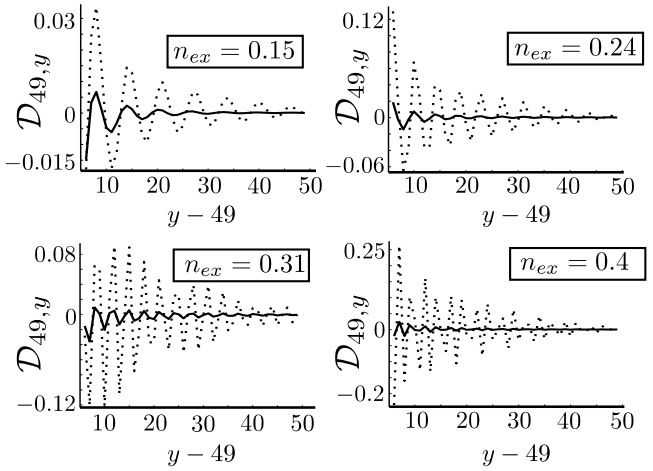


Figure 8. Representative examples of real-space density-density correlations for $J_p/J_h = 1$ (solid lines) and $J_p/J_h = 0.025$ (dotted lines) plotted from the center of a 96-site lattice. Here, $\mathcal{D}_{49,y} = \langle n_{49} n_y \rangle - \langle n_{49} \rangle \langle n_y \rangle$ is shown at four different ALE -densities for $U/|J_p| = 3$. At all densities, both amplitude and rate of decay of these DD-correlations are significantly improved by hopping imbalance over the case of $J_p = J_h$. The overall magnitude of the correlations increases with n_{ex}. Meanwhile, pairing correlations start to decay rapidly in this regime of $U/|J_p|$, see figure 7. Taken together, this identifies the regime of $|J_h/J_p| \ll 1$, $U/|J_p| = 2 - 3$ and $n_{ex} \geq 0.3$ as the region where the crystaline characteristics of the ALEs are most pronounced.

$K_c > 1$. The value of J_h/J_p where $K_c = 1$ will generally depend on the exciton density n_{ex}. Based on the value of K_c a phase diagram can be drawn, c.f. figure 1 in [40].

3.3. Phases of tightly bound ALEs

As ALEs map onto an attractive Hubbard model with imbalanced hopping of particles and holes, there are also some previously known results for case of isotropic hopping $J_p^1 = J_p^2 = J_p^3 = J_p$, yielding the phase diagram in the tightly bound limit $|J_p|/U, |J_h|/U \ll 1$. Here ALEs can be described as hard-core bosons with hopping rate J_{eff} and repulsive nearest-neighbour interactions V_{eff}. For a regular square or cubic lattice, mean-field calculations (c.f. e.g. [39]) predict either a checkerboard 'crystaline' Charge-Density-Wave (CDW) or a superfluid order at maximal density $n_{ex} = \frac{1}{2}$, depending on the value of V_{eff}/J_{eff}. The CDW is characterised by (DLRO), as was the exciton crystal studied in the previous section. Away from maximal filling, $n_{ex} < \frac{1}{2}$, mean-field calculations predict a supersolid phase - the coexistence of superfluid and crystaline order - for a broad range of n_{ex} (c.f. figure 4 in [39]). Beyond this range of densities, pure superfluidity is predicted. However, Quantum Monte-Carlo simulations [51, 52, 53, 54] show the prediction of a supersolid away from commensurability to be inaccurate for regular lattices. Depending on V_{eff}/J_{eff} and n_{ex}, tightly bound ALEs are either superfluid or undergo phase separation into spatially disjoint subsystems, one exhibiting superfluidity, the other checkerboard crystaline order §. Both Dynamical Mean Field Theory (DMFT) and standard mean-field calculations suggest [44] that when $J_p = J_h$ (i.e. $V_{eff}/J_{eff} = 1$) tightly bound ALEs will be superfluid at any density. One way to increase the value of $V_{eff}/J_{eff} = (J_p^2 + J_h^2)/(2J_pJ_h)$ and thereby attain phase separation beyond some critical n_{ex} is to have $J_p \neq J_h$ (c.f. [15]). The realization of ALEs proposed here will always have a significant imbalance, as the conduction band hopping rate typically surpasses that of valence band by an order of magnitude. Another possibility to increase the ratio V_{eff}/J_{eff} is to introduce additional nearest-neighbour interactions in the Hamiltonian (3) (see [39]), e.g. by considering fermionic dipolar molecules instead of atoms.

In summary, while for sufficiently low n_{ex}, tightly bound excitons always exhibit just superfluid order, exciton-exciton interactions can enhance density-density correlations. For larger values of n_{ex} and with hopping imbalance between particles and holes, they can result in phase-separation of the system into a checkerboard ALE-crystal and an ALE superfluid.

4. Probing atomic lattice excitons

Optical Lattice experiments provide a range of measurement possibilities that we can use to determine the characteristic properties of the many-body states that are produced. Three important examples of this for probing ALEs are Lattice modulation spectroscopy, RF Spectroscopy, and noise correlation measurements.

§ On triangular - and thus frustrated - lattices, Monte-Carlo simulations [56] have shown that a supersolid phase can appear however.

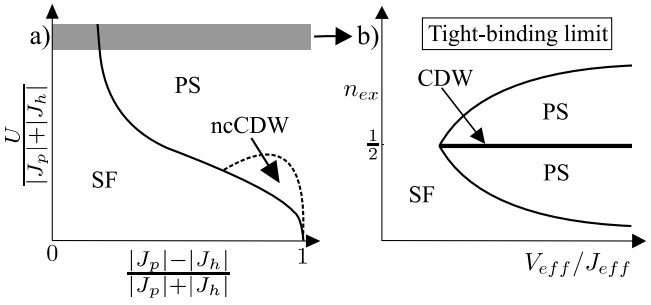


Figure 9. (a) Sketch of ALE phase diagram as a function of hopping imbalance and interaction strength relative to kinetic energy(after figure 2 in [44]). (b) Sketch of phase diagram for tightly bound ALEs at fixed density. SF: Superfluid, PS: Phase separation, CDW: checkerboard Charge-Density Wave, ncCDW: Charge-Density Wave at noncommensurate density. (a) Mean-field phase diagram for ALEs at fixed density close to $n_{ex} = \frac{1}{2}$. When the hopping imbalance $|J_p|-|J_h|/|J_p|+|J_h|$ is large enough, the superfluid phase-separates into superfluid and checkerboard-CDW. The separating line shifts with density. A pure non-checkerboard CDW-phase might also be possible in a small parameter range. For large $U/(|J_p|+|J_h|)$, ALEs become hard-core bosons with ranged interactions. (b) Sketch of a qualitative phase diagram for tightly bound ALEs. Doped away from the checkerboard CDW phase at $n_{ex} = \frac{1}{2}$, ALEs phase-separate into superfluid and checkerboard CDW, if V_{eff}/J_{eff} is large enough. This ratio can be tuned by changing J_h/J_p or by introducing longer-ranged interactions between particles and holes.

4.1. Exciton detection via lattice modulation

Periodic modulation of the lattice depth has become a standard way to probe the excitation spectrum of many-body systems on an optical lattice [55]. It is usually applied to systems in the groundstate. If the frequency of the modulation matches that of an excitation of the system, it drives transitions to higher-energy states. Such a transition is then detected by ramping down the confining potentials/interactions adiabatically, thereby transferring all potential energy into kinetic energy of the expanding atom cloud, which is then measured. This method has also been used to drive transition from excited states to lower energy states recently, in order to determine the energy of pairs of atoms bound together by on-site repulsion [17].

Qualitatively, probing for excitons via lattice modulations should show a pronounced decrease in the systems total energy around a frequency given by the bandgap minus the binding energy of the exciton.

4.2. Measuring the exciton condensate fraction via RF-spectroscopy

In order to demonstrate particle-hole pairing and in particular to detect the macroscopic occupation of the exciton groundstate, it is possible to employ a range of measuring techniques that have been developed for cold atoms experiments. At zero temperature, with no thermal excitation of collective exciton modes with $\mathbf{K} \neq \mathbf{w}$, the pairing amplitude Δ^P is directly proportional to the condensate fraction. It can be probed by the application of RF-spectroscopy, following the example of [57] (c.f. [58] for an experimental application). An RF-pulse with frequency ω_{RF} is used to couple the conduction band atoms, at energy ω_c, to another internal state with energy ω_3, with a detuning $\delta = \omega_{RF} - (\omega_3 - \omega_c)$, c.f. figure 10. Choosing $\delta > 0$, the particle-hole

pairs are broken up in this process. It is assumed that this state is still lattice-confined, with single particle energy $\xi^{(3)}_{\mathbf{k}} = \varepsilon^{(3)}_{\mathbf{k}} - \mu_{3,eff}$, where $\varepsilon^{(3)}_{\mathbf{k}}$ is the dispersion relation of the state on the lattice and $\mu_{3,eff}$ is the effective chemical potential, i.e. the chemical potential including any mean-field shift from interactions.

The RF-pulse with frequency ω_{RF} has an amplitude Ω that can be assumed to be slowly varying on length scales of the lattice. The transfer rate into the third state as a function of the RF-detuning, $I(\delta)$, can be calculated by generalizing the results in [57] to the case of ALEs with anisotropic conduction band hopping J^d_p (and therefore $E^{(1)}_{\mathbf{k}} \neq E^{(2)}_{\mathbf{k}}$). The result (at zero temperature) then becomes

$$I(\delta) = -2\pi|\Omega|^2 \sum_{\mathbf{k}} v^2_{\mathbf{k}} \delta(\xi^{(3)}_{\mathbf{k}} + \tilde{\Delta} + E^{(2)}_{\mathbf{k}})\theta(\xi^{(3)}_{\mathbf{k}}). \tag{38}$$

Here, $\tilde{\Delta} = \mu_3 - \mu_c - \delta$, and $\delta = \omega_{RF} - (\omega_3 - \omega_c)$ denotes the detuning of the RF-pulse from the transition frequency between the two internal states. μ_c is the chemical potential of the conduction band atoms, for which relation $\mu_c + \mu_h = \mu_{ex}$ holds. This expression is then valid generally for any J_p and J_h, assuming positive detuning.

The spectrum described by (38) has a gap, given by the minimum value of the δ-function argument. Its value is $\delta_{gap} = \varepsilon^{(3)}_0 + \min_{\mathbf{k}} E^P_{\mathbf{k}} - \mu_c$, assuming the additional internal state is initially unpopulated and does not scatter off the other states, i.e $\mu_{3,eff} = \mu_3 = 0$. If n_{ex} is known, Δ^P can be determined selfconsistently from δ_{gap} using (35).

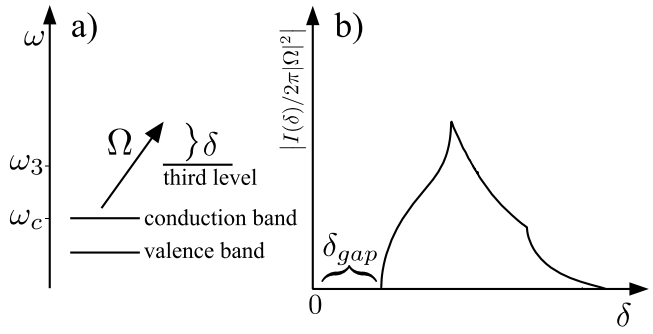


Figure 10. RF spectroscopy for an ALE condensate. (a) Excitation with RF-coupling Ω and detuning δ between conduction band atoms and a third internal state. (b) Transfer rate $|I(\delta)/2\pi\Omega^2|$ over detuning δ for $U/|J_p| = -8$, $U/|J_h| = -40$, $n_{ex} = 0.3$. The gap in the spectrum δ_{gap} is given by $\varepsilon^{(3)}_0 + \min_{\mathbf{k}} E^{(2)}_{\mathbf{k}} - \mu_c$. The kinks result from van Hove singularities.

4.3. Detecting crystal structure and pairing correlations via noise spectroscopy

We can detect both crystal structure and pairing correlation of ALEs using atom shot-noise measurements, a technique that was proposed in [35] and has been demonstrated in the laboratory [36, 37]. The former can be identified through second-order correlation functions of valence-band atoms, and the latter from second-order correlation functions of atoms in two bands. Each of these can be obtained from fluctuations in the density profile of the atomic gas.

For the ALE crystal, we expect holes to be anticorrelated with each other around the Fermi-edge. As the operators $b^\dagger_{\mathbf{k}}$ for valence-band atoms in are related to the

hole operators through $b^\dagger_{\mathbf{k}} = d_{-\mathbf{k}}$, we thus likewise expect an anticorrelation peak around the Fermi-edge for the valence-band atoms. In the case of the ALE-condensate, which is characterised by the pairing of particles and holes at opposite quasimomenta, pronouced anticorrelation of conduction- and valence-band atoms should be visible at equal quasimomentum around the Fermi-edge, i.e. "antipairing".

To obtain the density profiles experimentally, and from them the fluctuations, the Brillouin zones need to be imaged, i.e. lattice quasimomentum $\mathbf{k}$ needs to be mapped to real space position $\mathbf{R}(\mathbf{k})$ on the detector. This is achieved by ramping down the lattice sufficiently slowly to keep the atoms within their respective bands whilst preserving their quasimomentum (c.f. [13]). Valence-band atoms then occupy the first, and conduction-band atoms the second Brillouin zone (c.f. figure 11a and 13a). If density fluctuations are just limited by shot noise, density fluctuations of conduction and valence band atoms will be correlated according to the connected correlation function

$$\mathcal{G}_{cv}(\mathbf{R},\mathbf{R}') = \langle n^c_{\mathbf{R}(\mathbf{k})} n^v_{\mathbf{R}(\mathbf{k}')}\rangle - \langle n^c_{\mathbf{R}(\mathbf{k})}\rangle\langle n^v_{\mathbf{R}(\mathbf{k}')}\rangle, \tag{39}$$

whereas the density-fluctuations of valence-band atoms are correlated amongst themselves according to

$$\mathcal{G}_{vv}(\mathbf{R},\mathbf{R}') = \langle n^v_{\mathbf{R}(\mathbf{k})} n^v_{\mathbf{R}(\mathbf{k}')}\rangle - \langle n^v_{\mathbf{R}(\mathbf{k})}\rangle\langle n^v_{\mathbf{R}(\mathbf{k}')}\rangle. \tag{40}$$

Here $n^c_{\mathbf{R}(\mathbf{k})} = c^\dagger_{\mathbf{R}(\mathbf{k})} c_{\mathbf{R}(\mathbf{k})}$ and $n^v_{\mathbf{R}(\mathbf{k}')} = b^\dagger_{\mathbf{R}(\mathbf{k}')} b_{\mathbf{R}(\mathbf{k}')}$.

For the case of ALEs in 1D we used the numerical algorithm employed in section 3.2 to compute both correlation functions in different parameter regimes. These are plotted in Figs. 11 and 12, which when contrasted display the crystal and superfluid characteristics of the system in different parameter regimes. figure 11a shows the momentum-space density profile for excitons in the first and second Brillouin zones for the example of a parameter regime where we expect a crystal to form. The fluctuations that would occur in the experimental measurement of this density profile can be used to compute the second order correlation functions (39) and (40) [35]. Figure 11b depicts $\mathcal{G}_{cv}(R,R')$, that results from Brillouin-zone resolved measurement, for different system parameters. It shows how antipairing is suppressed when n_{ex} increases and $U/|J_p|$ decreases. Figure 12 shows the periodic dips at $G \pm n_{ex}\pi/a$ in $\mathcal{G}_{cv}(R,R')$ (where G is any reciprocal lattice vector). This can be measured from the noise correlations measured from real momentum distributions, as is done in switching off the lattice suddenly, analogous to previous experiments [36, 37]. The periodic anti-correlations indicate the crystal, and their locations relative to the large positive correlations reflect the reciprocal lattice vector of the exciton crystal. Dips appear here because we are computing noise correlations for fermions [35]. Taken together, the figures further illustrate the analysis of section 3.2. They show that pairing and density-density correlations are complementary, with pairing being strongly suppressed and density-density correlations around the Fermi-edge enhanced in the limit of strong hopping imbalance and $n_{ex} \approx \frac{1}{3}$, $U/|J_p| = 2-3$. This indicates onset of the exciton crystal. Paring increases and the dips in the density-density correlations vanish when n_{ex} decreases or J_h/J_p increases, corresponding to the dominance of superfluid character in the system.

For higher dimensional systems, the existence of a pure crystal phase is not resolved, though crystal and superfluid order can coexist (see sec. 3.3). When only

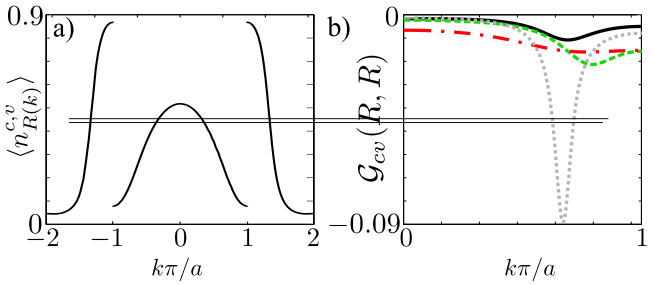


Figure 11. (a) Density profile for quasimomentum states in the first two Brillouin zones for 1D ALEs, calculated for a 40-site lattice in the crystal regime ($n_{ex} = \frac{13}{40}$, $U/|J_p| = 4$, $J_h/J_p = 0.025$). (b) Pairing anticorrelations at $k = k'$ between conduction- and valence-band atoms in different parameter regimes on a 40-site lattice. With parameters such that we expect to observe an ALE crystal (solid line, $n_{ex} = \frac{13}{40}$, $U/|J_p| = 4$, $J_h/J_p = 0.025$), antipairing is strongly supressed as compared to a system outside this regime (other lines), with a minimum at the Fermi-edge, $n_{ex}\pi/a$ away from the minimum of the Bloch band at π/a. For equal hopping (dotted line, $n_{ex} = \frac{13}{40}$, $U/|J_p| = 4$, $J_h/J_p = 1$) antipairing is strong and dominant (see figure 12). At lower densities (dashed line, ($n_{ex} = \frac{9}{40}$, $U/|J_p| = 4$, $J_h/J_p = 1$) antipairing is still stronger than for the cystal, with the minimum shifted due to lower density. For increased attraction (dash-dotted line, $n_{ex} = \frac{13}{40}$, $U/|J_p| = 10$, $J_h/J_p = 1$) antipairing is slightly increased over the crystal

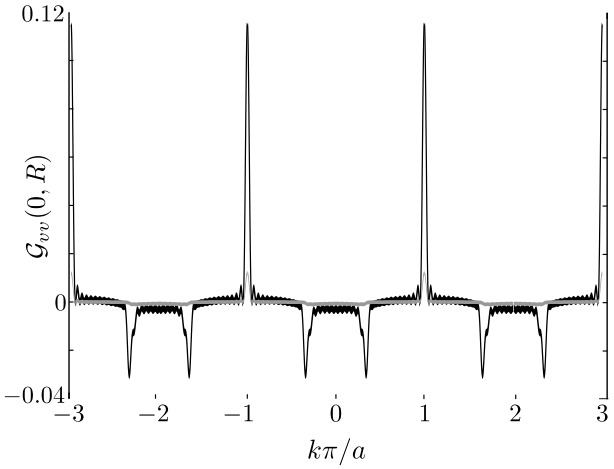


Figure 12. Second order correlation function for valence band atoms, computed on a 40-site lattice. These represent results that can be obtained from noise correlation measurements, in which the crystal structure of ALEs appears. In the appropriate regime (black line, $n_{ex} = \frac{13}{40}$, $U/|J_p| = 4$, $J_h/J_p = 0.025$), dips appear at $\pm n_{ex}\pi/a$ away from the location of reciprocal lattice vectors corresponding to the optical lattice. These signalize the formation of the ALE crystal, as holes become localized through atom-mediated long-range repulsions (see figure 4), and occur at momentum values corresponding to the reciprocal lattice vector of the exciton crystal. Such a result is representative of the crystal regime. If we increase $U/|J_p|$ to 10 (not shown), the dip visibility decreases only slightly, and the crystal structure still appears. Increasing J_h/J_h to 1 (grey line) causes the crystal and thus the dips to disappear, as does decreasing n_{ex} to $\frac{9}{40}$ (not shown)

superfluid order is present, the correlations between conduction- and valence-band atoms $\mathcal{G}_{cv}(\mathbf{R},\mathbf{R}')$ can be expressed through the mean-field coefficients u and v:

$$\mathcal{G}_{cv}(\mathbf{R},\mathbf{R}') = \begin{cases} -u^2_{\mathbf{R}(\mathbf{k})}v^2_{\mathbf{R}(\mathbf{k})} & \mathbf{R}(\mathbf{k}) = \mathbf{R}(\mathbf{k}') \\ 0 & \mathbf{R}(\mathbf{k}) \neq \mathbf{R}(\mathbf{k}') \end{cases} . \tag{41}$$

An example plot of the column-integrated correlation function contained in the shot noise is shown in figure 13b. Considering that the correlation at $\mathbf{k} = \mathbf{k}'$ equals $u^2_{\mathbf{k}}v^2_{\mathbf{k}}$

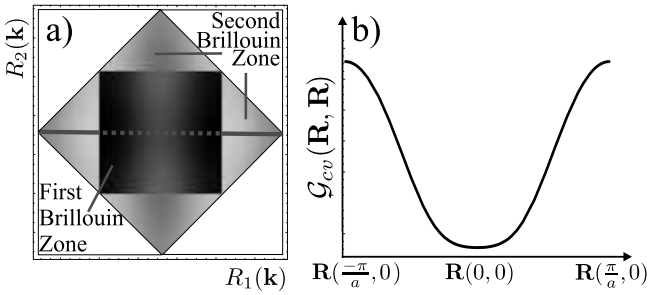


Figure 13. (a) Calculated density profile of conduction and valence band atoms as they would appear after ideal time-of-flight imaging. Dark areas denote high atom density. The third dimension is column-integrated. The first and second Brillouin zone are mapped to real-space positions for the condensate ground state with $n_{ex} = 0.3$, $U/|J^1_p| = -8$, $J^2_p/J^1_p = J^3_p/J^1_p = -0.5$, $U/|J_h| = -40$. (b) Calculated example of noise correlations between conduction and valence band atoms, at positions $\mathbf{R}(\mathbf{k}) = \mathbf{R}(\mathbf{k}')$. Here $\mathbf{R}(\mathbf{k})$ is taken along the dotted line in figure a, and $\mathbf{R}(\mathbf{k}')$ is taken along the solid line. The anticorrelation of conduction and valence band atoms is most pronounced around the Fermi-edge of atoms and holes. As $J^1_p < 0$, $J^2_p, J^3_p > 0$, the Fermi-edge in figure a lies along the k_2 axis. The anticorrelation appears reduced because of density-integration along $\mathbf{R}(0,0,k_3)$.

in the mean-field theory, this approach provides an alternative for determining the condensate fraction via the definition of Δ^P.

5. Exciton Formation in an Optical Lattice

5.1. General remarks

One method to prepare excitons in an optical lattice would be to create a band insulator of spin polarised fermions in the valence band, and then to excite atoms to the conduction band, using, e.g., a Raman transition. This would be most directly analogous to the method by which excitons are produced in the context of solid state systems.

However, in the context of Atomic lattice excitions, it would be desirable both to have control over the number of excitons produced, and to have a means of producing these excitons in the lowest possible many-body energy state. In contrast to excitons in the solid state, the weak coupling of Atomic lattice excitions to dissipative processes means that excitons prepared with a significant energy above that of the groundstate will not be naturally cooled to this state. As a consequence, particle-hole pairs cannot be created in an arbitrary manner if the ground state is the desired outcome.

5.2. A preparation scheme

One scheme that we have investigated in detail for its efficiency in preparing a many-exciton state close to the condensate groundstate is a melting scheme adapted from [59]. Through adiabatic tuning of the system parameters, a chosen filling factor of ALEs can be prepared at essentially $T = 0$ (this is in the same spirit as other adiabatic preparation proposals, such as [60]).

We begin with a spin-polarised Fermi gas loaded into an optical lattice with an applied superlattice, which gives certain lattice sites an offset energy V. The initial configuration of atoms is loaded so that the lowest motional state in each lattice site is occupied, as well as the first excited state in wells with lower energy, as shown in figure 14a. This can be achieved, e.g., using the methods discussed in [59, 61, 62]. The final filling factor is chosen by the periodicity of the superlattice with respect to the basic lattice period. In each case, we will want to generate at some point an interaction energy U between atoms in the first excited motional level and atoms in the ground motional level.

This can be achieved, e.g., by introducing an off-resonant Raman coupling between the initial internal state of the spin-polarised fermions and a second internal state. If the detuning is chosen so that atoms in the excited motional level in the initial internal state are coupled to the second internal state near to resonance with the first motional level, then the coupling will be much further detuned for the atoms in the initial internal state in the lowest band than for those in the upper band. This will produce a different admixture of the second internal state for atoms in each band, and the non-identical internal states will allow s-wave interactions between atoms in different bands.

A simple scheme for the adiabatic formation of excitons is now the following: (i) Atoms are removed from the lowest motional level in sites containing two atoms, by transferring them to a different internal state and removing them from the lattice (see figure 14b-I). This is possible because the resonant energy of the transition to a different internal state is shifted by differences in interaction energies, and because it is possible to address different bands using spin-dependent lattices for the initial and final states of the transfer [59]. (ii) The interaction U is "switched on". (iii) V is adiabatically decreased to zero, effectively melting the preformed excitons and forming the desired exciton gas (see figure 14c).

Until the last step, the state is protected by a gap of order V, but the last step must be performed adiabatically with respect to the exciton tunnelling rate, which for $J_p, J_h \ll U$ can be estimated as $J_{ex} \approx 2J_pJ_h/U$.

These timescales can be improved upon by slightly modifying the above scheme. Instead of removing atoms initially in step (i), V is adiabatically decreased to zero, forming the ground state for delocalised fermions in the first Bloch band, as shown in figure 14b-II. If the lattice depth is then suddenly increased to a large value where $J_p, J_h \approx 0$ and atoms then removed as in (i), then we preform the ground state of hard-core excitons. If we then switch on the interaction U and adiabatically decrease the lattice depth, we obtain the desired exciton ground state. Note that in this scheme we must take care of the sign of the effective hopping for excitons, which in some cases requires an additional complication. The atoms that we delocalise in the first step should have the same hopping rate as the composite exciton. Thus, for J_p, $J_h < 0$, and $U > 0$, we obtain $J_{ex} > 0$, and therefore atoms should first be delocalised in the lowest band, then transferred to the upper band whilst the lattice is very deep.

This requires atoms to be initially loaded in two internal states to allow for double occupation in the lowest band.

The advantages of the latter scheme are clear from figure 15, where we show the energy of the final state in 1D as a function of ramp speed in the final step. We produce a final state with 15 excitons on 60 lattice sites, with $U/|J_p| = U/|J_h| = 20$, by ramping V and then J on a timescale given in units of $J_{\rm final}^{-1}$. These results were computed using a time-dependent DMRG algorithm [45, 46, 47, 48], and show clearly that ramping on a timescale much smaller than that implied by $2J_pJ_h/U$ produce states with energies very near the ground state (indicated by the dashed line in the figure). The main curve shows the result for adiabatic ramping in the last step beginning from the grounds state of hard core atoms in single atoms, and the inset shows the energy of a single atom state after a similar ramp.

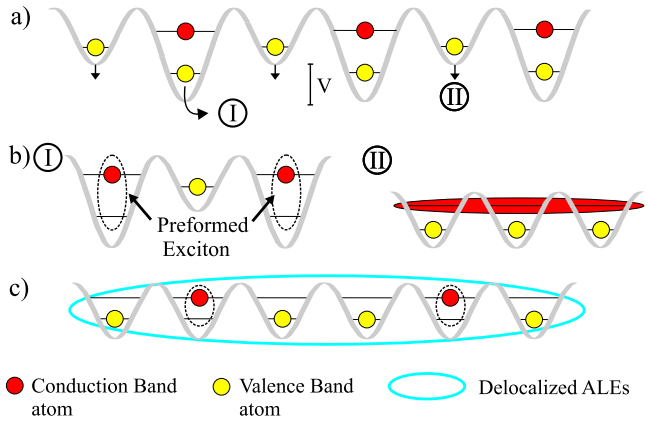


Figure 14. Melting scheme to obtain an ALE condensate. (a) Initially the ground state is formed in the presence of a superlattice, giving site offsets V. Two alternative melting schemes, I and II, proceed from there. I: (b) ALEs are preformed locally by removal of the atom in the lower motional state on doubly occupied sites. c) Melting the state by ramping V down adiabatically yields delocalised ALEs. II) (b) Groundstate of delocalised fermions in the upper band is formed, melting the initial state by adiabatically decreasing V. (Depending on sign of the hopping for ALEs, this must be done in the lower band instead, see text for details) (c) The resulting state is frozen by ramping up the lattice suddenly, and atoms in the lowest band are removed from doubly occupied sites. This automatically pairs each atom in the upper band with a hole in the lower band, in the localised state expected in the limit $U/J \to \infty$. Ramping the lattice down adiabatically then yields ALEs close to the ground state.

6. Summary and Outlook

Excitons are composite objects of fundamental interest in the context of semiconductor physics. However, the theoretical models presented for these systems relate even more closely to the situation we discuss in optical lattices, making ALEs an important testbed for study of the most interesting properties of these objects. In particular, the availability of techniques for state preparation and measurement in optical lattices provide tools to study excitons that strongly completment those available in semiconductor systems. ALEs can also be realised in parameter regimes that strongly contrast with those available in semiconductors. In this way we not only obtain the

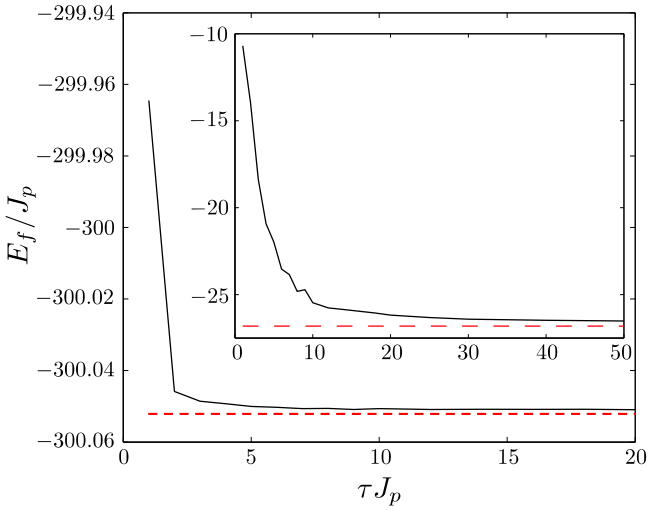


Figure 15. Results of the Melting scheme II, as depicted in figure 14. Main graph shows final state energy E_f/J_p obtained from numerical calculation of decreasing U/J for ALEs that were preformed utilizing the groundstate of delocalised atoms (see figure 14b-II, c). Parameters are: 60 sites, 15 ALEs, $U/|J_p| = U/|J_h| = 20$. Exact groundstate energy is indicated through a dashed red line. The inset shows E_f/J for the preparation of the groundstate of free atoms in the upper band from the intial band insulator (see figure 14a, b-II), for identical parameters. Exact groundstate energy is indicated by dashed red line.

possibility for condensation of these objects, but also for preparation of additional phases, including an exciton crystal. Optical Lattices also provide the possibility to directly reduce the dimensionality of the system, making the important case of 1D excitons directly accessible.

There are several open paths for the study of ALEs. Firstly, many of the results we have discussed in this work, particularly pertaining to the exciton crystal could be generalised to 2D and 3D. The structure of degenerate excited bands [27] could also be introduced as an extra element in the higher dimensional context. In addition, the study of composite objects could be developed in the direction of multiple bound ALEs, in the case that, e.g., attractive interactions are generated between excitons. Other possibilities also arise to study systems analogous to excitonium (see [2], ch. 10), a dynamically created collection of excitons that exists in the limit where the gap between valence of conduction-band is small compared with the atom-atom interactions.

As a final comment, it is clear that there is a strongly connection between ALEs and superconductivity or superfluidity of fermions via the attractive Hubbard model, which we obtain here for interacting particles and holes. It would also be possible to consider the case of repulsive interactions between particles and holes, in which case one could obtain repulsively bound ALEs, in the sense that the two particle bound state appears above the scattering continuum. The model describing this system would be a Hubbard model with repulsive interations, which may lead to interesting analogies with d-wave pairing states.

Acknowledgments

The authors acknowledge insightful discussions with H. P. Büchler, M. Combescot, and M. Szymanska. A. K. would like to thank T. Giamarchi for helpful discussions on the hopping-imbalanced Hubbard model and Luttinger liquids. Work in Innsbruck was supported by Austrian Science Foundation (FWF), and by the European Commission through the Integrated Project FET/QIPC SCALA. This work was supported by Academy of Finland (project number 213362) and conducted as part of a EURYI scheme award. See www.esf.org/euryi.

Appendix A. Solution for the Single Exciton

As for the COM-motion, (6) with $U = 0$ corresponds to a Schrödinger equation for a free particle on a lattice. That equation is resolved by the Green's function with discrete translation invariance,

$$G_0(r - r') = a \int_{-\pi/a}^{\pi/a} \frac{\mathrm{d}k}{2\pi} \frac{\exp\left[\mathrm{i}k(r - r')\right]}{E + 2J\cos(ka) + \mathrm{i}\eta}. \tag{A.1}$$

For $U > 0$ - the single particle motion with an impurity at lattice-site $r = 0$ - the Kroneker-delta in (6) allows an easy, explicit resummation of the recursive relation for the full Green's function:

$$\Rightarrow G(r, r') = G_0(r - r') + \frac{G_0(r)G_0(r')}{1 - G_0(0)/U} \tag{A.2}$$

One can read off from this expression that the full Green's function has a single bound state pole for each value of K with energy E_K, where the denominator of the second term vanishes, i.e., for $U^{-1} = G_0(0)$. The numerator yields directly the unnormalised bound state wavefunction in relative coordinates, $\rho_r = CG_0(r)$, which is given by

$$\rho_r = Ca \int_{-\pi/a}^{\pi/a} \frac{\mathrm{d}k}{2\pi} \frac{\exp\left[\mathrm{i}kr\right]}{E + 2J\cos(ka)} \tag{A.3}$$

where C is the normalisation constant. This is depicted in figure 2 a,b. The dispersion relation E of the exciton, which forms the exciton solution in figure 2 is determined by the implicit equation

$$U^{-1} = a \int_{-\pi/a}^{\pi/a} \frac{\mathrm{d}k}{2\pi} \frac{1}{E + 2J\cos(ka)}, \tag{A.4}$$

which can be integrated to give the result quoted in section 2.1.

Appendix B. Solution to the N-impurities problem

In solving the Schrödinger equation for ALEs in the Born-Oppenheimer (BO) approximation, we must treat the problem of N spin-polarised fermions on a lattice (the conduction band atoms), moving in a potential provided by the N holes, which essentially act as impurities. The BO Hamiltonian from (12) can be decomposed into a sum of single-atom Hamiltonians $h_n[\underline{\mathbf{R}}]$. As atom-hole interaction is on-site, we can write

$$H_{BO}[\underline{\mathbf{R}}] = \sum_{n=1}^{N} h_n[\underline{\mathbf{R}}], \quad h_n[\underline{\mathbf{R}}] = -J_p\widetilde{\Delta}_{\mathbf{r}_n} - U\sum_{n'=1}^{N} \delta_{\mathbf{r}_n\mathbf{R}_{n'}} \tag{B.1}$$

Each of the single-atom Hamiltonians $h[\underline{\mathbf{R}}]$ has eigenstates $\rho_k(\mathbf{r};\underline{\mathbf{R}})$, obtained from the solving the eigenvalue equations

$$h[\underline{\mathbf{R}}]\rho_k(\mathbf{r};\underline{\mathbf{R}}) = E_k[\underline{\mathbf{R}}]\rho_k(\mathbf{r};\underline{\mathbf{R}}) \tag{B.2}$$

where k runs over all bound and scattering solutions. In general, depending on dimensionality and the ratio of U/J_p, there will be up to N bound state solutions for N holes for any configuration $\underline{\mathbf{R}}$. If the impurities approach each other too closely (on a length scale dependent on $U/|J_p|$), some of the bound states will disappear. In the following, we assume that the system is sufficiently dilute, that N bound states will always exist. For $N = 2$ this will always be the case provided $U/|J_p| \gtrsim 2$.

From the $\rho_k(\mathbf{r};\underline{\mathbf{R}})$'s, the exact many-atom wavefunctions $\phi_\alpha(\underline{\mathbf{r}};\underline{\mathbf{R}})$, can be constructed by forming the Slater determinant:

$$\phi_\alpha(\underline{\mathbf{r}};\underline{\mathbf{R}}) = \begin{vmatrix} \rho_{k_1}(\mathbf{r}_1;\underline{\mathbf{R}}) & \dots & \rho_{k_1}(\mathbf{r}_N;\underline{\mathbf{R}}) \\ \vdots & \ddots & \vdots \\ \rho_{k_N}(\mathbf{r}_1;\underline{\mathbf{R}}) & \dots & \rho_{k_N}(\mathbf{r}_N;\underline{\mathbf{R}}) \end{vmatrix} \tag{B.3}$$

The wavefunction $\phi_\alpha(\underline{\mathbf{r}};\underline{\mathbf{R}})$ is antisymmetric in $\underline{\mathbf{r}}$ and solves (15). The index α thus is a multiindex, with $\alpha = (k_1, \dots, k_N)$ and the condition $k_a \neq k_b$, for $a \neq b$, and the BO-energies $E_{\alpha;BO}$ of (15) are obtained from summing the single-atom energies:

$$E_{\alpha;BO}[\underline{\mathbf{R}}] = \sum_{\{k_1,\dots,k_N\}=\alpha} E_{k_a}[\underline{\mathbf{R}}] \tag{B.4}$$

We can then obtain the explicit form of the single-atom wavefunctions $\rho_k(\mathbf{r};\underline{\mathbf{R}})$, i.e. the solutions to (B.2). As the single atom Green's function $G(\mathbf{r}',\mathbf{r};\underline{\mathbf{R}})$ has the spectral decomposition $G(\mathbf{r}',\mathbf{r};\underline{\mathbf{R}}) = \sum_k \rho_k^*(\mathbf{r}';\underline{\mathbf{R}})\rho_k(\mathbf{r};\underline{\mathbf{R}})/(E - E_k[\underline{\mathbf{R}}] + \imath\eta)$, (we do not write the E-dependence of the Green's function explicitly in the following), knowing $G(\mathbf{R}_n,\mathbf{r};\underline{\mathbf{R}})$ gives access to both eigenenergies $E_k[\underline{\mathbf{R}}]$ and wavefunctions (from poles and residues respectively).

As the full single atom wavefunction obeys

$$G(\mathbf{r}',\mathbf{r};\underline{\mathbf{R}}) = G_0(\mathbf{r}',\mathbf{r}) + \sum_{\mathbf{r}'} G_0(\mathbf{r}',\mathbf{r}')V(\mathbf{r}')G(\mathbf{r}',\mathbf{r};\underline{\mathbf{R}}) \tag{B.5}$$

where $V(\mathbf{r}') = -U\sum_{n=1}^N \delta_{\mathbf{r}'\mathbf{R}_n}$ and

$$G_0(\mathbf{r}',\mathbf{r}) = a^D \int_{B.Z.} \frac{\mathrm{d}^D k}{(2\pi)^D} \frac{\exp\left[\mathrm{i}\mathbf{k}(\mathbf{r}'-\mathbf{r})\right]}{E + 2J_p\sum_d \cos(k_d a) + \mathrm{i}\eta}. \tag{B.6}$$

The set of $G(\mathbf{R}_n,\mathbf{r};\underline{\mathbf{R}})$'s can be determined from the linear system of equations

$$\mathbf{A}[E,\underline{\mathbf{R}}]\mathbf{G}(\mathbf{r};\underline{\mathbf{R}}) = \mathbf{G}_0(\mathbf{r}), \tag{B.7}$$

where

$$(\mathbf{A}[E,\underline{\mathbf{R}}])_{nm} = \begin{cases} 1 + UG_0(\mathbf{R}_m,\mathbf{R}_m) & m = n \\ UG_0(\mathbf{R}_n,\mathbf{R}_m) & m \neq n \end{cases} \tag{B.8}$$

and $\mathbf{G}(\mathbf{r};\underline{\mathbf{R}}) = (G(\mathbf{R}_1,\mathbf{r};\underline{\mathbf{R}}),\dots,G(\mathbf{R}_N,\mathbf{r});\underline{\mathbf{R}})$, $\mathbf{G}_0(\mathbf{r}) = (G_0(\mathbf{R}_1,\mathbf{r}),\dots,G_0(\mathbf{R}_N,\mathbf{r}))$. The eigenenergies are determined from the condition

$$\det(\mathbf{A}[E_k[\underline{\mathbf{R}}],\underline{\mathbf{R}}]) = 0 \tag{B.9}$$

and we assume here that this has N bound-state solutions. We thus see immediately that any N-hole single-atom bound state wavefunction can always be written as a linear combination of functions that have the form of single-hole bound states.

For example, for $N = 2$ (B.7) is solved by

$$G(\mathbf{R}_1, \mathbf{r}; \underline{\mathbf{R}}) = \frac{(1 + UG_0(\mathbf{R}_1, \mathbf{R}_1))G_0(\mathbf{R}_1, \mathbf{r}) - UG_0(\mathbf{R}_1, \mathbf{R}_2)G_0(\mathbf{R}_2, \mathbf{r})}{(1 + UG_0(\mathbf{0}, \mathbf{0}))^2 - U^2 G_0^2(\mathbf{R}_1, \mathbf{R}_2)} \tag{B.10}$$

$$G(\mathbf{R}_2, \mathbf{r}; \underline{\mathbf{R}}) = \frac{(1 + UG_0(\mathbf{R}_2, \mathbf{R}_2))G_0(\mathbf{R}_2, \mathbf{r}) - UG_0(\mathbf{R}_1, \mathbf{R}_2)G_0(\mathbf{R}_1, \mathbf{r})}{(1 + UG_0(\mathbf{0}, \mathbf{0}))^2 - U^2 G_0^2(\mathbf{R}_1, \mathbf{R}_2)} \tag{B.11}$$

where the eigenenergies $E_\pm[\mathbf{R}_1, \mathbf{R}_2]$ are implicitly determined from the denominator being zero,

$$(1 + UG_0(\mathbf{0}, \mathbf{0}))^2 = U^2 G_0^2(\mathbf{R}_1, \mathbf{R}_2), \tag{B.12}$$

and the residue yields two wavefunctions,

$$\rho_\pm(r; \underline{\mathbf{R}}) = C(G_0(R_1, \mathbf{r}) \pm G_0(R_2, \mathbf{r})), \tag{B.13}$$

where C carries the normalization.

The lowest energy BO-potential is given by $E_+[\mathbf{R}_1, \mathbf{R}_2] + E_-[\mathbf{R}_1, \mathbf{R}_2]$, examples of which are plotted in figure 4 for the 1D case.

Appendix C. Description of a many-exciton condensate

The condensed state of the excitons, in which a macroscopic number of them occupies the single-exciton groundstate, breaks the symmetry of the Hamiltonian associated with number conservation. Macroscopic occupation of the groundstate $A_0^\dagger = \sum_k A_{0,0}(\mathbf{k}, -\mathbf{k}) c_\mathbf{k}^\dagger d_{-\mathbf{k}}^\dagger |0\rangle$ implies that $\langle c_\mathbf{k}^\dagger d_{-\mathbf{k}}^\dagger \rangle \neq 0$. A way to introduce symmetry breaking into the Hamiltonian is by applying a Bogoliubov canonical transformation to the particle and hole operators [1, 2]:

$$C_\mathbf{k} = \mathcal{D} c_\mathbf{k} \mathcal{D}^\dagger = u_\mathbf{k} c_\mathbf{k} + v_\mathbf{k} d_{-\mathbf{k}}^\dagger \tag{C.1}$$

$$D_\mathbf{k} = \mathcal{D} d_\mathbf{k} \mathcal{D}^\dagger = u_\mathbf{k} d_\mathbf{k} - v_\mathbf{k} c_{-\mathbf{k}}^\dagger \tag{C.2}$$

with $u_\mathbf{k}^2 + v_\mathbf{k}^2 = 1$ to maintain anti-commutation relations. Here $C_\mathbf{k}$, $D_\mathbf{k}$ correspond to new quasiparticle and quasihole operators, that have vanishing occupation number in the condensate groundstate of the system,

$$\langle C_\mathbf{k}^\dagger C_\mathbf{k} \rangle = \langle D_\mathbf{k}^\dagger D_\mathbf{k} \rangle = 0, \tag{C.3}$$

which automatically imposes $\langle c_\mathbf{k}^\dagger d_{-\mathbf{k}}^\dagger \rangle \neq 0$. Inserting the inverse of (C.1) into (22) and rearranging to obtain a normal-ordered form again, the Hamiltonian decomposes into a sum of three terms:

$$H = H_{const} + H_2 + H_{Int} \tag{C.4}$$

These terms have the following structure:

- H_{const} is a constant containing no operators

- H_2 is given by

$$H_2 = \sum_\mathbf{k} E_\mathbf{k}^{(1)} C_\mathbf{k}^\dagger C_\mathbf{k} + E_\mathbf{k}^{(2)} D_\mathbf{k}^\dagger D_\mathbf{k} - F_\mathbf{k} (C_\mathbf{k}^\dagger D_{-\mathbf{k}}^\dagger + D_{-\mathbf{k}} C_\mathbf{k}) \tag{C.5}$$

with

$$E^{(1)}_{\mathbf{k}} = E^p_{\mathbf{k}} u^2_{\mathbf{k}} - E^h_{\mathbf{k}} v^2_{\mathbf{k}} + \sum_{\mathbf{l}} \left[u^2_{\mathbf{k}} \left(V_0 + V^p_0 - V^p_{\mathbf{l}-\mathbf{k}} \right) + v^2_{\mathbf{k}} \left(V^h_{\mathbf{l}-\mathbf{k}} - V_0 - V^h_0 \right) \right] v^2_{\mathbf{l}} \\ -2u_{\mathbf{k}} v_{\mathbf{k}} \sum_{\mathbf{l}} V_{\mathbf{l}-\mathbf{k}} u_{\mathbf{l}} v_{\mathbf{l}} \tag{C.6}$$

$$E^{(2)}_{\mathbf{k}} = E^h_{\mathbf{k}} u^2_{\mathbf{k}} - E^p_{\mathbf{k}} v^2_{\mathbf{k}} + \sum_{\mathbf{l}} \left[u^2_{\mathbf{k}} \left(V_0 + V^h_0 - V^h_{\mathbf{l}-\mathbf{k}} \right) + v^2_{\mathbf{k}} \left(V^p_{\mathbf{l}-\mathbf{k}} - V_0 - V^p_0 \right) \right] v^2_{\mathbf{l}} \\ -2u_{\mathbf{k}} v_{\mathbf{k}} \sum_{\mathbf{l}} V_{\mathbf{l}-\mathbf{k}} u_{\mathbf{l}} v_{\mathbf{l}} \tag{C.7}$$

$$F_{\mathbf{k}} = u_{\mathbf{k}} v_{\mathbf{k}} \left[E^p_{\mathbf{k}} + E^h_{\mathbf{k}} - \sum_{\mathbf{l}} \left(2V_0 + V^p_0 + V^h_0 - V^p_{\mathbf{l}-\mathbf{k}} - V^h_{\mathbf{l}-\mathbf{k}} \right) v^2_{\mathbf{l}} \right] \\ + \left(u^2_{\mathbf{k}} - v^2_{\mathbf{k}} \right) \sum_{\mathbf{l}} V_{\mathbf{l}-\mathbf{k}} u_{\mathbf{l}} v_{\mathbf{l}} \tag{C.8}$$

The last term in (C.5) corresponds to a process where electron-hole pairs with total momentum equal to zero are being spontaneously created from and annihilated into the condensate.

- H_{Int} is the transformed interaction part of the Hamiltonian and contains all possible quartic combinations of particle and hole operators. Among other processes, these correspond to the creation and annihilation of two pairs of quasiparticles and quasiholes with total momentum zero.

H re-expressed in the new operators can thus be unstable with respect to the spontaneous creation and annihilation of free quasiparticle-quasihole pairs. To rectify this, Keldysh and Kozlov demand that $u_{\mathbf{k}}$ and $v_{\mathbf{k}}$ be chosen such that they satisfy the constraint [1]

$$\langle C^\dagger_{\mathbf{k}} D^\dagger_{-\mathbf{k}} \rangle = \langle C_{\mathbf{k}} D_{-\mathbf{k}} \rangle = 0. \tag{C.9}$$

The average here is performed over the exact groundstate, and thus $u_{\mathbf{k}}$ and $u_{\mathbf{k}}$ need to be determined from the full transformed Hamiltonian, subject to (C.9), which is a difficult task.

It is simpler to satisfy constraint (C.9) just for the groundstate of H_2 and disregard H_{Int} for the moment. This is equivalent to demanding that $F_{\mathbf{k}} = 0$ for all $\mathbf{k}$ [2], which in turn is equivalent to $u_{\mathbf{k}}$ and $v_{\mathbf{k}}$ satisfying mean-field (26) - (27). In this approximation, only particle-hole pairs at opposite momenta are correlated. The Bogoliubov transformation that generates these correlations is

$$\mathcal{D} = \exp \left[\sqrt{n_{ex}} \sum_{\mathbf{k}} A(\mathbf{k}) (c^\dagger_{\mathbf{k}} d^\dagger_{-\mathbf{k}} - d_{-\mathbf{k}} c_{\mathbf{k}}) \right] \tag{C.10}$$

where $u_{\mathbf{k}} = \cos(\sqrt{n_{ex}} A(\mathbf{k}))$, $v_{\mathbf{k}} = \sin(\sqrt{n_{ex}} A(\mathbf{k}))$. When applied to the vacuum particle-hole vacuum $|0\rangle$, $\mathcal{D}$ generates the coherent state to the operators $c^\dagger_{\mathbf{k}} d^\dagger_{-\mathbf{k}}$, $d_{-\mathbf{k}} c_{\mathbf{k}}$ which automatically satisfies (C.3) and (C.9). The new groundstate is consequently given by

$$|\psi\rangle = \mathcal{D}|0\rangle = \prod_{\mathbf{k}} (u_{\mathbf{k}} + v_{\mathbf{k}} c^\dagger_{\mathbf{k}} d^\dagger_{-\mathbf{k}}) |0\rangle, \tag{C.11}$$

of the same form as the BCS-groundstate. The dispersion relations of the single-quasiparticle excitations above this groundstate are given by (C.6) and (C.7).

References

[1] Keldysh L V and Kozlov A N 1968 *JETP* **27** 521
[2] Moskalenko S A and Snoke D W 2000 *Bose-Einstein Condensation of Excitons and Biexcitons*, (Cambridge: Cambridge University Press)
[3] Hanamura E and Haug H 1977 *Phys. Rep.* **33**, 209
[4] Griffin A, Snoke D W, Stringari S (eds.) 1995 *Bose-Einstein Condensation* (Cambridge: Cambridge University Press)
[5] Kasprzak J *et al* 2006 *Nature* **443** 409
[6] Snoke D W 2002 *Science* **298** 1368
[7] Balili R, Hartwell V, Snoke D W, Pfeiffer L and West K 2007 *Science* **316** 1007
[8] Levitov L S, Simons B D and Butov L V 2005 *Phys. Rev. Lett.* **94** 176404
[9] Combescot M, Betbeder-Matibet O and Combescot R *Preprint* arXiv:0706.2419v1
[10] Combescot M, Betbeder-Matibet O and Dubin F *Phys. Rep.* in press
[11] Chin J K, Miller D E, Liu Y, Stan C, Setiawan W, Sanner C, Xu K and Ketterle W 2006 *Nature* **443** 961
[12] Rom T, Best T, van Oosten D, Schneider U, Fölling S, Paredes B and Bloch I 2006 *Nature* **444** 733
[13] Köhl M, Moritz H, Stöferle T, Günter K and Esslinger T 2005 *Phys. Rev. Lett.* **94** 080403
[14] Ospelkaus S, Ospelkaus C, Wille O, Succo M, Ernst P, Sengstock K and Bongs K 2006 *Phys. Rev. Lett.* **96** 180403
[15] Lee C 2004 *Phys. Rev. Lett.* **93** 120406
[16] Jaksch D and Zoller P 2005 *Annals of Physics* **315** 52
[17] Winkler K, Thalhammer G, Lang F, Grimm R, Hecker-Denschlag J, Daley A J, Kantian A, Büchler H P and Zoller P 2006 *Nature* **441** 853
[18] Bloch I, Dalibard J and Zwerger W *Preprint* arXiv:0704.3011v1
[19] Lewenstein M, Sanpera A, Ahufinger V, Damski B, Sen De A and Sen U 2007 *Advances in Physics* **56** 243
[20] Greiner M, Mandel O, Esslinger T, Hänsch T W and Bloch I 2002 *Nature* **415** 39
[21] Stöferle T, Moritz H, Schori C, Köhl M and Esslinger T 2004 *Phys. Rev. Lett.* **92** 130403
[22] Fallani L, Lye J E, Guarrera V, Fort C and Inguscio M 2007 *Phys. Rev. Lett.* **98** 130404
[23] Spielman I B, Phillips W D and Porto J V 2007 *Phys. Rev. Lett.* **98** 080404
[24] Sanpera A, Kantian A, Sanchez-Palencia L, Zakrzewski J and Lewenstein M 2004 *Phys. Rev. Lett.* **93** 040401
[25] Micheli A, Brennen G K and Zoller P 2006 *Nature Physics* **2** 341
[26] Scarola V W and Das Sarma S 2005 *Phys. Rev. Lett.* **95** 033003
[27] Liu W V and Wu C 2006 *Phys. Rev.* A **74** 013607
[28] Duan L M, Demler E and Lukin M D 2003 *Phys. Rev. Lett.* **91** 090402
[29] Garcia-Ripoll J J, Martin-Delgado M A and Cirac J I 2004 *Phys. Rev. Lett.* **93** 250405
[30] Santos L, Baranov M A, Cirac J I, Everts H U, Fehrmann H and Lewenstein M 2004 *Phys. Rev. Lett.* **93** 030601
[31] Koehler T, Goral K and Julienne P S 2006 *Rev. Mod. Phys.* **78** 1311
[32] Donley E A, Claussen N R, Thompson S T and Wieman C E 2002 *Nature* **417** 529
[33] Loftus T, Regal C A, Ticknor C, Bohn J L and Jin D S 2002 *Phys. Rev. Lett.* **88** 173201
[34] Theis M, Thalhammer G, Winkler K, Hellwig M, Ruff G, Grimm R and Hecker-Denschlag J 2004 *Phys. Rev. Lett.* **93** 123001
[35] Altman E, Demler E and Lukin M D 2004 *Phys. Rev.* A **70** 013603
[36] Fölling S, Gerbier F, Widera A, Mandel O, Gericke T and Bloch I 2005 *Nature* **434** 481
[37] Greiner M, Regal C A, Stewart J T and Jin D S 2005 *Phys. Rev. Lett.* **94** 110401
[38] Wouters M and Orso G 2006 *Phys. Rev.* A **73** 012707
[39] Micnas R, Ranninger J and Robaszkiewick S 1990 *Rev. Mod. Phys.* **62** 113
[40] Cazalilla M A, Ho A F, Giamarchi T 2005 *Phys. Rev. Lett.* **95** 226402
[41] Comte C and Nozières P 1982 *J. Physique* **43** 1069
[42] Nozières P and Schmitt-Rink S 1985 *J. Low. Temp. Phys.* **59** 195
[43] Fetter A L and Walecka J D 2003 *Quantum Theory of Many-Particle Systems* (New York: McGraw-Hill)
[44] Dao T, Georges A and Capone M *Preprint* arXiv:0704.2660v1
[45] Vidal G 2003 *Phys. Rev. Lett.* **91** 147902
[46] Vidal G 2004 *Phys. Rev. Lett.* **93** 040502
[47] Daley A J, Kollath C, Schollwöck U and Vidal G 2004 *J. Stat. Mech.:* Theor. Exp. P04005
[48] White S R and Feiguin A E 2004 *Phys. Rev. Lett.* **93** 076401

[49] Giamarchi T 2004 *Quantum Physics in One Dimension* (Oxford: Oxford Science Publications)
[50] Noack R M, White S R and Scalapino D J 1996 *Physica* C **270** 281
[51] Batrouni G G and Scalettar R T 2000 *Phys. Rev. Lett.* **84** 1599
[52] Hebert F, Batrouni G G, Scalettar R T, Schmid G, Troyer M and Dorneich A 2001 *Phys. Rev.* B **65** 014513
[53] Kohno M and Takahashi M 1997 *Phys. Rev.* B **56** 3212
[54] Kuklov A, Prokofev N and Svistunov B 2004 *Phys. Rev. Lett.* **93** 230402
[55] Schori C, Stöferle T, Moritz H, Köhl M and Esslinger T 2004 *Phys. Rev. Lett.* **93** 240402
[56] Wessel S and Troyer M 2005 *Phys. Rev. Lett.* **95** 127205
[57] Törmä P and Zoller P 2000 *Phys. Rev. Lett.* **85** 487
[58] Chin C, Bartenstein M, Altmeyer A, Riedl S, Jochim S, Hecker-Denschlag J and Grimm R 2004 *Science* **305** 1128
[59] Rabl P, Daley A J, Fedichev P O, Cirac J I and Zoller P 2003 *Phys. Rev. Lett.* **91** 110403
[60] Trebst S, Schollwöck U, Troyer M and Zoller P 2006 *Phys. Rev. Lett.* **96** 250402
[61] Viverit L, Menotti C, Calarco T and Smerzi A 2004 *Phys. Rev. Lett.* **93** 110401
[62] Griessner A, Daley A J, Jaksch D and Zoller P 2005 *Phys. Rev.* A **72** 032332
[63] Isacsson A and Girvin S M 2005 *Phys. Rev.* A **72** 053604